AUS DEM LEHRSTUHL FÜR NEUROCHIRURGIE
PROF. DR. NILS OLE SCHMIDT
DER FAKULTÄT FÜR MEDIZIN
DER UNIVERSITÄT REGENSBURG

Dielektrische Eigenschaften von intrakraniellen Tumoren zur Verbesserung der Behandlung von Glioblastomen mit elektrischen Wechselfeldern (TTFields)

Inaugural – Dissertation
zur Erlangung des Doktorgrades
der Medizin

der
Fakultät für Medizin
der Universität Regensburg

vorgelegt von
Rana Tahir Rasool

2023

AUS DEM LEHRSTUHL FÜR NEUROCHIRURGIE
PROF. DR. NILS OLE SCHMIDT
DER FAKULTÄT FÜR MEDIZIN
DER UNIVERSITÄT REGENSBURG

Dielektrische Eigenschaften von intrakraniellen Tumoren zur Verbesserung der Behandlung von Glioblastomen mit elektrischen Wechselfeldern (TTFields)

Inaugural – Dissertation
zur Erlangung des Doktorgrades
der Medizin

der
Fakultät für Medizin
der Universität Regensburg

vorgelegt von
Rana Tahir Rasool

2023

Dekan:	Prof. Dr. Dirk Hellwig
1. Berichterstatter:	Prof. Dr. Martin Proescholdt
2. Berichterstatter:	Prof. Dr. Peter Hau
Tag der mündlichen Prüfung:	18.09.2023

Table of Contents

1. Abstract

Glioblastoma (GBM) is the most common and most aggressive form of primary brain tumor. In newly diagnosed GBM patients, despite utilizing the tri-modality treatment approach, including neurosurgical resection, radiotherapy and chemotherapy with TMZ, the median survival time is only 14.6 months. The recurrence rate of GBM is very high, and the prognosis after recurrence is extremely poor. TTFields is a novel treatment method that uses alternating electric fields of 200 kHz to interrupt tumor cell mitosis and induce cell death. A prospective randomized-phase 3 trial (EF-14) evaluated the use of TTFields with TMZ in newly diagnosed GBM, and demonstrated a 3 months longer PFS and OS as compared to controls. The efficacy of TTFields depends on the level of compliance or device “on-time”, and its intensity (1 to 3 V/cm) in the tumor tissue. The intensity of TTFields in the tumor tissue is influenced by its conductivity and permittivity. The ability of a material to orient dipole in repose to an electric field is permittivity and the ability to move charges is conductivity. The permittivity of a material opposes the applied electric field. The electric field intensity in a material is inversely proportional to its conductivity. The conductivity and permittivity for GBM at 200 kHz are unknown. In this study, conductivity and permittivity of GBM tissue were measured from patients who went under surgical resection. It was measured *in vitro* by utilizing the parallel-plates method and the E4980AL Precision LCR meter. The mean conductivity of GBM was 0.353 (S/m) with SD of 0.133 and mean permittivity was 3896.778 Farad/m with SD of 2461.872. This study showed a high inter- / intraindividual variability in conductivity and permittivity of GBM. Histological analysis demonstrated that low myelin content and higher cellularity was linked to higher conductivity. The dielectric properties of GBM tissue from this study could be used for more effective treatment planning with TTFields. This study also suggests to obtain values from each individual patient due to high inter- and intra-heterogeneity in dielectric properties of GBM. Moreover, our study design provides a reliable method to investigate the dielectric properties of healthy and tumor tissues in a laboratory setting.

1. Abstrakt

Das Glioblastom (GBM) ist die häufigste und aggressivste Form eines primären Hirntumors. Bei neu diagnostiziertem GBM beträgt die mediane Überlebenszeit trotz des trimodalen Behandlungsansatzes, der eine neurochirurgische Resektion, Strahlentherapie und Chemotherapie umfasst, nur 14,6 Monate. Die Rezidiv-Rate des GBM ist sehr hoch und die Prognose nach einem Rezidiv ist extrem schlecht. TTFields ist eine neuartige Behandlungsmethode, bei der elektrische Wechselfelder von 200 kHz eingesetzt werden, um die Mitose der Tumorzellen zu unterbrechen und den Zelltod herbeizuführen. In einer klinischen Phase-3-Studie wurde der Einsatz von TTFields in Kombination mit TMZ bei neu diagnostiziertem GBM untersucht und dabei ein um drei Monate längeres PFS und OS im Vergleich zu den Kontrollen nachgewiesen. Die Wirksamkeit von TTFields hängt vom Grad der Compliance oder der "On-Time" des Geräts und seiner Intensität (1 bis 3 V/cm) im Tumorgewebe ab. Die Intensität der TTFields im Tumorgewebe wird durch dessen Leitfähigkeit und Permittivität beeinflusst. Die Fähigkeit eines Materials, Dipole in Ruhe auf ein elektrisches Feld auszurichten, ist die Permittivität, die Fähigkeit, Ladungen zu bewegen, die Leitfähigkeit. Die Permittivität eines Materials wirkt dem angelegten elektrischen Feld entgegen. Die Stärke des elektrischen Feldes in einem Material ist umgekehrt proportional zu seiner Leitfähigkeit. Die Leitfähigkeit und Permittivität von GBM bei 200 kHz sind unbekannt. In dieser Studie wurden Leitfähigkeit und Permittivität von GBM-Gewebe von Patienten gemessen, die sich einer chirurgischen Resektion unterzogen. Die Messung erfolgte in vitro mit der Parallelplattenmethode und dem E4980AL Precision LCR-Meter. Die mittlere Leitfähigkeit von GBM lag bei 0,353 (S/m) mit einem SD von 0,133 und die mittlere Permittivität bei 3896,778 Farad/m mit einem SD von 2461,872. Diese Studie zeigte eine hohe inter- / intraindividuelle Variabilität in der Leitfähigkeit und Permittivität von GBM. Die histologische Analyse zeigte, dass ein geringer Myelingehalt und eine höhere Zellularität mit einer höheren Leitfähigkeit verbunden waren. Die dielektrischen Eigenschaften von GBM-Gewebe aus dieser Studie könnten für eine effektivere Behandlungsplanung mit TTFields genutzt werden. Diese Studie legt auch nahe, Werte von jedem einzelnen Patienten zu erhalten, da die dielektrischen Eigenschaften von GBM stark inter- und intraheterogen sind. Darüber hinaus bietet unser Studiendesign eine zuverlässige Methode zur Untersuchung der dielektrischen Eigenschaften von gesundem und Tumorgewebe in einem Labor.

2. Introduction

2.1 Glioblastoma

2.1.1 Epidemiology

Malignant gliomas are the most common primary malignant brain tumors and accounts for 80% of all brain tumors [1]. Annual incidence rate of malignant glioma per 100,000 inhabitants in United States is 5.26 [2] and in Europe 4.8 [3]. Glioblastoma (GBM) is the most common and most aggressive form of primary brain tumor, accounting for approximately 80% of all malignant gliomas [2]. The incidence rises accordingly with increasing age, the incidence is 11.6 per 100,000 inhabitants after the age of 60 [3], and it is expected to increase with the ageing of the population [4]. It is more common in males than females with a gender ratio of 3:2 [5]. Caucasians have higher tendency to develop malignant glioma as compared to African or Asian population [6]. Early diagnosis and treatment of malignant glioma do not improve outcomes, excluding the usefulness of screening for this disease [4].

2.1.2 Etiology

Malignant glioma develops in a multistep process due to genetic changes that can result from intrinsic and environmental factors. Patients suffering from rare hereditary syndromes including Cowden, Turcot, Li-Fraumeni, neurofibromatosis type 1 and type 2, tuberous sclerosis, and familial schwannomatosis can develop malignant glioma [7]. Genome-wide association studies have suggested that presence of multiple susceptibility genes within one patient can likely develop malignant glioma [8]. A family history of glioma is associated with a 2-fold increase in the risk of developing glioma [4]. A high exposure of ionizing radiation is an established environmental risk factor to develop glioma, while atopic diseases such as asthma, eczema, and hay fever reduces the risk [9, 10].

2.1.3 Molecular classification

According to the new WHO Classification of Tumors of the central nervous system (CNS) a glioblastoma is diagnosed in the setting of an IDH-wildtype diffuse and astrocytic glioma in adults with microvascular proliferation or necrosis or TERT promoter mutation or EGFR gene amplification or + 7/− 10 chromosome copy number changes [11]. The O6-methylguanine-DNA-methyltransferase (MGMT) gene in glioblastoma is

most frequently determined in clinical practice because of its relevance for prognosis and therapy [12]. MGMT is one of the DNA repair genes that can remove the alkyl group that is therapeutically induced by chemotherapy agents such as temozolomide [12, 13]. MGMT is methylated in an average of 40% of newly diagnosed glioblastomas [14]. MGMT methylation leads to longer progression-free and median overall survival and a better treatment response to temozolomide in older patients [15-17].

2.1.4 Histopathology and tumor cell invasion

GBM is has an extensive heterogeneous histopathology. The histopathological features of GBMs are atypia, mitotic activity, increased cellular density, microvascular proliferation and necrosis with or without cellular pseduopalisading [18]. GBM is highly invasive and infiltrate the surrounding brain tissue in a diffuse pattern, yet confined to the central nervous system (CNS); only 0.2% of all cases metastasize [19].

At cellular level, pseudopalisades play an important role in this aggressively progressive growth pattern. The dense, columnar, cellular formations around the necrotic tumor parts, which are pathognomonic for glioblastoma, are referred to as pseudopalisades. There are a number of hypothesis about the nature of pseudopallisading cells. One is that these are probably migrating cells that move away from the area of perivascular tumor hypoxia due to vaso-occlusion of the supplying vessels [20]. The vaso-occlusion probably arises because of epithelial apoptosis and intravascular thrombosis due to blood coagulation proteins such as tissue factor or plasminogen activator inhibitor-1 secreted by the tumor cells. Non-migrating cells die because of hypoxia, which leads to central necrosis. In response to hypoxia, the pseudopalisades overexpress hypoxia-inducing factor (HIF) -1α, which upregulates the transcription of vascular endothelial growth factor (VEGF) and thus causes an excessive proangiogenic response with microvascular proliferation in regions peripheral to the central hypoxia as well as migration to the newly formed vessels. Pseudopalisades also activate proteins such as matrix metalloproteinases, which further promote cell migration from the affected vessels into the surrounding brain tissue [20-22].

GBM invasion results from a continuous bidirectional interaction between tumor cells and their microenvironment [23]. The tumor cells can migrate to other parts of the brain and tend to cross the contralateral hemisphere by orienting themselves to the structures of neuropil, which can give rise to additional tumor foci; a complete microscopic

resection therefore can never be achieved and remnant tumor cells are frequent cause of disease recurrence [24]. Unfortunately, current standard therapies are unable to target infiltrative tumor cells [24].

2.1.5 Clinical presentation

Headaches are the most frequent symptom, present in about 50% of cases, at the time of diagnosis, and in a nonspecific pain pattern [25]. However, a tumor-associated headache can be distinguished due to its progressive severity, unilateral localization, worsening with bending over, presence of nausea or vomiting and new-onset in a patient older than 50 years [4, 25]. Seizures with focal onset are reported to be the presenting manifestations in about 20% to 40% of patients [26]. Other symptoms depending on tumor location and size can include hemiparesis, sensory loss and visual disturbance, gait imbalance and incontinence. In older patients cognitive difficulties, personality changes and language difficulties can be present which could be mistaken for psychiatric disorders or dementia [4].

2.1.6 Diagnosis

The diagnostic method of choice for GBM is brain magnetic resonance imagining (MRI) with and without contrast [27]. CT scan is performed for those patients, with pacemakers, who are unable to undergo MRI. GBM shows enhancement with gadolinium and may have central areas of necrosis; peri-tumor white matter edema is usually present which can be seen in fluid attenuated inversion recovery (FLAIR) MRI. Findings on MRI can be indistinguishable from brain metastases [4]. Further, some non-neoplastic syndromes, including brain abscess, subacute stroke and inflammatory diseases, may mimic findings of GBM neuroimaging; therefore, patient's history and alternative diagnosis are vital to rule out these syndromes before surgery [28].

2.1.7 Treatment

Patients with suspected GBM undergo surgical resection to relieve mass effect, and providing tissue for histologic and molecular tumor characterization. In inoperable tumors, stereotactic biopsy may be performed for histological diagnosis.

2.1.7.1 Surgical resection

The aim of GBM surgery should be to maximize the extent of resection without causing new neurological deficits and maintaining a good quality of life for patients [29]. The

extent of resection (EOR) has been reported to be the leading prognostic factor for enhanced survival in patients when the EORs range 70–98% [30]. Multiple lesions, “butterfly” GBM, anatomical limitations, tumor volume of ≥30 mL and leptomeningeal dissemination are challenging conditions for total resection in clinical practice [30-33] (2-5). There is no consensus on the definition of gross total resection of GBM (1). Gross total resection can be defined as the removal of all the tumor, as detected by magnetic resonance imaging whether on T2WI or FLAIR [34]. Extending the tumor resection could be considered by performing awake craniotomies with additional imaging adjuncts like the intraoperative MRI, ultrasound, and 5-ALA guidance [35]. However, despite these intraoperative technologies that allow real-time visualization of tumor borders, a clear differentiation between the normal brain and the residual tumor continues to be a major challenge [36].

2.1.7.2 Radiation and chemotherapy

After surgical resection of the newly diagnosed GBM, adjuvant radiotherapy combined with chemotherapy is main treatment option for newly diagnosed GBM. The typical radiotherapy dose is 60Gy divided in 30 fractions. The use of intensity modulated radiotherapy has been increasingly preferred because of better targeting capability, but to date there is no evidence of superiority over other focal radiotherapy techniques. Because GBM is a diffusely infiltrative disease, there is currently no defined role for stereotactic radiosurgery or brachytherapy as part of first-line treatment [37].

The DNA alkylating agent, temozolomide (TMZ), is given orally due to its good bioavailability, concomitantly with radiotherapy, followed by an adjuvant course. The findings of a randomized phase 3 trial supported the use of this regimen that showed the addition of temozolomide increased the median survival to 15 months vs 12 months with radiotherapy alone; the 2-year survival rate was 27% vs 10%, respectively [38]. A post hoc tissue analysis suggested that the patients with methylated MGMT promoter had more benefit from the addition of temozolomide to radiotherapy [15]. However, optimal treatments for elderly patients and patients with poor performance status remain to be established, although radiotherapy alone and temozolomide alone have both been shown effective and well tolerated [39-41].

In addition to TMZ, biodegradable polymers containing the alkylating agent carmustine is also approved by the US Food and Drug Administration (FDA) as first-line treatment.

This agent can be implanted into the tumor bed as biodegradable discs (Gliadel) after tumor resection. However, a phase 3 trial has suggested a modest survival benefit [42], but methodological problems with study design and occurrence of frequent toxicities, such as brain edema, infection, and seizures, precluded wide adoption of this treatment [4]. Lomustine is another alkylating nitrosourea compound, which is a highly lipid-soluble drug, thus it crosses the blood-brain barrier. Therefore unlike carmustine, lomustine is administered orally. Despite somewhat prolonged progression-free survival, treatment with lomustine plus anti–VEGF therapy with bevacizumab did not confer a survival advantage over treatment with lomustine alone in patients with progressive glioblastoma [43].

After first-line treatment, virtually all glioblastoma patients experience disease progression after a median PFS of 7 to 10 months [44]. Unfortunately, survival is not improved with currently available salvage treatments and only subset of patients has benefited from such treatments. In recurrent GBM, surgical resection may be considered for mass effect relief, and updating histology and molecular characteristics of the tumor, although survival benefits are unclear. However, for a majority of patients, surgery will not be indicated because of tumor location, widespread disease in the brain, or the patient's poor physical performance status [4].

Salvage chemotherapy options include bevacizumab, TMZ, and other alkylating agents, such as nitrosoureas and procarbazine. In the USA, bevacizumab is frequently used treatment for recurrent glioblastoma. Although a clinical trial has not shown survival benefits of the drug, but it has symptomatic treatment benefit of reducing the peritumoral edema due to VEGF, and it facilitates corticosteroid taper [45, 46]. Metronomic TMZ dosing schedules, given at lower doses for extended period, is another salvage therapy option with a better toxicity profile, which may be particularly helpful in patients who have completed the adjuvant TMZ and experience recurrence while not receiving treatment [47-49]. Regorafenib is an oral multikinase inhibitor of angiogenic, stromal, and oncogenic receptor tyrosine kinases. A randomised, multicentre, open-label phase 2 trial showed an encouraging overall survival benefit of regorafenib in recurrent glioblastoma [50].

2.1.8 Prognosis

GBM is a devastating brain tumor with poor prognosis despite advances in surgery, radiation, and chemotherapy. Many factors influence the outcome of GBM treatment. One of these factors is Karnofsky performance status (KPS), which is a measurement of the ability of cancer patients to perform ordinary tasks. The KPS scores ranges from 0 to 100, and a higher score means the patient is better able to carry out daily activities. The other factors that determine the prognosis of a GBM patient include age, the extent of resection or tumor size, morphological, histological and genetic characteristics, such as MGMT promoter methylation status [51]. The factors associated with improved survival are age < 65 years, tumor size >2 cm, radical tumor resection, MGMT promotor methylation status, KPS score <60 [52].

In newly diagnosed GBM patients, despite utilizing the tri-modality treatment approach, including neurosurgical resection, radiotherapy and chemotherapy with TMZ, the median survival time is only 14.6 months, overall survival at 2 years is only 27.2%, and a 5-year survival rate is of about 9.8% [38, 53]. The prognosis without any treatment is even more abysmal. Further, the recurrence rate of GBM is very high, and the prognosis after recurrence is extremely poor, with very short PFS and OS [54, 55].

2.2 What are tumor treating fields (TTFields)?

TTFields is a novel treatment method that uses alternating electric fields of intermediate frequency to interrupt tumor cell mitosis and induce cell death. It has been approved by the FDA for treatment of both newly diagnosed and recurrent GBM. In Germany its use is restricted to the newly diagnosed GBM. TTFields with TMZ is indicated for the newly diagnosed, supratentorial GBM after surgical resection independent from the extent of resection, and completion of radiation therapy with concomitant standard of care chemotherapy [56]. In clinical trials, TTFields showed better efficacy in newly diagnosed GBM. On the other side it showed similar efficacy in recurrent GBM as compared to the available investigators choice of therapy [57]. Further, TTFields treatment has better toxicity profile with improved patient-reported quality of life as compared to the standard treatments chemotherapy [56, 57].

2.2.1 Preclinical studies of TTFields

The role of low-intensity, intermediate-frequency, alternating electric fields that are delivered by means of insulated electrodes, as a therapeutic option for treating malignant tumors was first evaluated in preclinical studies. Kirson et al. showed that the TTFs effectively inhibit the growth of various human and rodent tumor cell lines *in vitro* and *in vivo* [58]. This effect of TTFs was shown to be non-thermal, selectively affecting the dividing cells and maximal cytotoxic effect was achieved when the electric fields were applied parallel to the axis of cell division [59]. Further, two modes of actions of TTFs were demonstrated: inhibition of cell proliferation and destruction of cells while undergoing division [58]. Based on their ability to kill tumor cells in culture, these alternating electric fields were referred to as tumor treating fields (TTFields).

The antitumor effects of TTFs in glioma was confirmed in an *in vivo* study, where intracranial rat gliomas were treated with TTFs, 200 kHz at intensity of 1 to 3 V/cm, and tumor volume reductions were observed, compared with untreated tumors. Further, it was shown that periodically switching the electric field between two orthogonal field directions was 20% more effective compared to applying in a single direction; for glioma cells, the inhibition of cell division was frequency and dose-dependent at 200 kHz in the range of 1 to 3 V/cm [59].

2.2.2 Clinical studies of TTFields

The encouraging preclinical studies led to preliminary evaluation of TTFields in patients with recurrent GBM. In first pilot trial TTFields as monotherapy was examined in 10 patients with recurrent, TMZ-refractory GBM, comparing time to PFS and OS with historical controls [59]. The patients treated with TTFs had PFS time of 26.1 weeks, compared with 9.5 weeks for historical controls, and a median OS of 62.2 weeks, compared with 29.3 weeks for historical controls. Further, 67.5% of the TTFs treated patients with recurrent high-grade gliomas were still alive 1 year after initiating the therapy [59]. TTFields were tested in a second pilot trial consisting of 20 concurrent newly diagnosed GBM patients who received initial therapy, including surgical resection, radiotherapy and TMZ [60]. TTFields plus TMZ was compared with TMZ alone as maintenance therapy. The PFS time with TTFs plus TMZ was 155 weeks versus 31 weeks with TMZ alone in the concurrent historical control group. Median OS was >39 months in the patients treated with adjuvant TTFs plus TMZ as compared to 14.7 months in a

matched historical control group treated with adjuvant TMZ alone. The main side effect in patient treated with TTFields was grade I-II dermatitis [60].

In patients with recurrent GBM, a prospective, randomized, phase 3 EF-11 trial was conducted to compare TTFields as monotherapy with physician's choice of chemotherapy as monotherapy, or in combination with various agents including bevacizumab, irinotecan, nitrosurea, carboplatin, or TMZ [57]. The median age of patients in this trial was 54 years and median KPS of 80. Patients were instructed to wear the TTFields device $\geq$ 18 hours a day. The primary endpoint was OS, and secondary endpoints included PFS, PFS at 6 months, overall response rate, 1-year survival, safety and quality of life. The median survival of 6.6 months in the TTFs arm and 6.0 months in the physician's choice of chemotherapy arm was not significantly different. Patients treated with TTFs alone had comparable OS and PPF to that of patients who received physician's choice of chemotherapy. The median PFS of TTFields and physician's choice of chemotherapy was 2.2 months and 2.1, and the PFS at 6 months was 21.4% and 15.1% respectively. One-year survival was 20% in both treatment arms. However, patients randomized to the TTFields arm self-reported a higher quality of life, including improved cognitive and emotional functioning. On the other hand, patients treated with chemotherapy had statistically higher incidence of gastrointestinal, hematologic, and infectious adverse events. Severe adverse events also occurred less frequently in the TTFields-treated group (6%) as compared to the control (16 %). The most common device-related events experienced with TTFields therapy were mild to moderate scalp irritation beneath the arrays. These were managed with topical corticosteroids and periodic relocation of the arrays [57].

In a post-hoc analysis of the EF-11 trial, it was found out that the most significant predictor of response in the TTFs arm was treatment compliance [61]. The analysis showed that OS was significantly longer in patients whose time on therapy was 18 hours/day or greater (>75% compliance rate) than in those with less than 75% compliance rate (7.7 vs. 4.5 months). The antitumor effects of TTFields only occur when the device delivering them is actively in use. Unlike chemotherapy, there is no treatment related half-life that continues after initial administration. Hence, compliance is especially critical for the effectiveness of TTFs therapy.

The analyses also showed significantly higher median OS with TTFs versus control for patients with KPS >80, tumor size >18 cm^2, prior low grade glioma, and those who had previously failed bevacizumab therapy [61]. Further, use of dexamethasone had a profound effect on the median OS in both TTFields and control; however, it was more profound with TTFields treatment where subjects who used >4.1 mg/day dexamethasone had a markedly shortened mean OS of 4.8 months compared with those who received <4.1 mg/day (mean OS of 11.0 months) [62, 63]. In 2011, the US Food and Drug Administration (FDA) approved TTFields therapy for recurrent GBM, based largely on the results from the EF-11 trial showing equivalent efficacy as compared to control while with improved patient reported QoL and a lower incidence of serious adverse events with TTFields [64].

The impact of TTFs therapy in patients with recurrent GBM treated outside of clinical trials was examined using data from the Patient Registry Data set (PRiDe) [65]. PRiDe is a post marketing registry of all recurrent GBM patients treated with TTFs in clinical practice setting in the US between 2011 and 2013. The PRiDe data analyses showed that the median OS with TTFields was 9.6 months, significantly longer than the 6.6 months reported in the EF-11 trial. One and two-year OS rates were more than double for TTFs therapy patients as compared to the EF-11 trial (1-year: 44% vs. 20%; 2-year: 30% vs. 9%). Favorable prognostic factors for improved survival were first or second recurrence versus subsequent recurrence, higher KP status, and no prior bevacizumab use. The adverse effects were similar to the one found in EF-11 trial, with most common being skin toxicity in 24.3% patients [65].

A prospective randomized-phase 3 trial (EF-14) evaluated the use of TTFields in the initial management of newly diagnosed GBM [66]. In the trial patients who had completed chemo-radiotherapy were randomized to receive maintenance treatment with either TTFields plus TMZ or TMZ alone as standard adjuvant therapy. No placebo or sham device was used in this trial. The arms were well balanced in regard to age, performance status, resection, and MGMT promoter methylation. A pre-specified interim analysis performed after the first 315 patients reached a minimum follow up of 18 months showed efficacy with acceptable tolerability and safety. This led to early mandatory stoppage of the trial, as per the independent Data Safety Monitoring Committee’s recommendations.

The pre-specified interim analysis demonstrated a significantly longer median PFS in the TTFields arm versus control arm after a median follow up of 38 months (7.1 vs. 4 months). The median OS was 20.5 months in the TTFields arms versus 15.6 months in the control arm. The results for all the enrolled patients with a minimum follow-up of 18 months and median follow up of 36 months confirmed the results of the interim analysis that the addition of TTFs to TMZ confers greater benefit in PFS and OS than TMZ alone [56]. Further, three-quarters of the patients in this trial wore the device >18 hours per day on average during the first three months of therapy. The most common adverse event related to the device was skin irritation of grade 2 or 3, occurring in 43% of patients. Patients also reported grade 1 or 2 mild anxiety, confusion, insomnia and headaches, most commonly at the initiation of therapy [56]. The findings of this study led to the approval of TTFields by FDA in combination with TMZ for the treatment of newly diagnosed GBM in October 2015.

2.2.3 TTFields in clinical practice

TTFields are delivered by the Optune system called NovoTTF-200-A System (Figure 1). It consists of electric field generator, insulated transducer arrays, charger with spare batteries, carrying case and power outlet adapter, and it has total weight of approximately 1.2 kg [67]. The Optune system delivers TTFields to the region of the GBM tumor via 2 orthogonal pairs of transducers arrays placed on the shaved scalp of patients. One pair of arrays is placed on the left and right sides of the head (LR array), and the other pair on the anterior and posterior aspects of the head (AP array). Each transducer array is made of 9 ceramic disks arranged in 3x3 configuration, and these arrays are disposable and replaced every few days [68]. These two pairs of arrays are connected to an electric field generator, which is, in turn, either connected to a portable battery pack or a power cord that can be inserted directly into an electric outlet. The device delivers a maximum current of 2000 mA peak-to-peak at a frequency of 200 kHz. At any given instance, the current is delivered to only one pair of arrays, and the direction of the field is switched between a pair of arrays once per second. The level of current is adjusted to maintain a skin temperature below a critical level of 41°C. Skin temperature is measured by sensors located in the center of the electrodes' discs [69].

Figure 1: Components of the second generation Optune™ system (© Novocure Ltd).

Patients are treated outside the hospital environment, and prior to Optune treatment initiation, patients or caregiver are trained from a technical perspective by a Device Support Specialist from Novocure to correctly operate the device. The duration of Optune treatment should be monitored carefully as studies have indicated that approximately 15% of patients with recurrent GBM who ultimately show durable response exhibit initial tumor growth before tumor shrinkage [70]. Therefore, it is important to allow time when assessing the effectiveness of TTFields therapy in GBM and it should not be discontinued on the basis of early radiographic changes alone [70-72]. In general, the device is worn until second progression of the tumor in order to account for the transient initial enlargement of the tumor [64].

Patient therapy is personalized by configuring transducer array layout placement on the scalp of the patient using MRI measurements and the NovoTAL System. NovoTAL system is based on computational modeling that creates an array map on the basis of Patient's head anatomy and tumor size and location; this allows maximizing TTFields intensity to the tumor site [73]. Studies have indicated that there is increased delivery of TTFields to the tumor when arrays are adapted to the individual tumor location [74]. Although, such proprietary software was not utilized during the clinical trials of TTFields. The output of the NovoTAL system is a three-dimensional array layout map, which is used by the patient or caregiver in placing the arrays on the scalp during the

course of TTFields treatment. Figure 2 is taken from Riley et al. [75] and shows transducer array placement in a GBM patient.

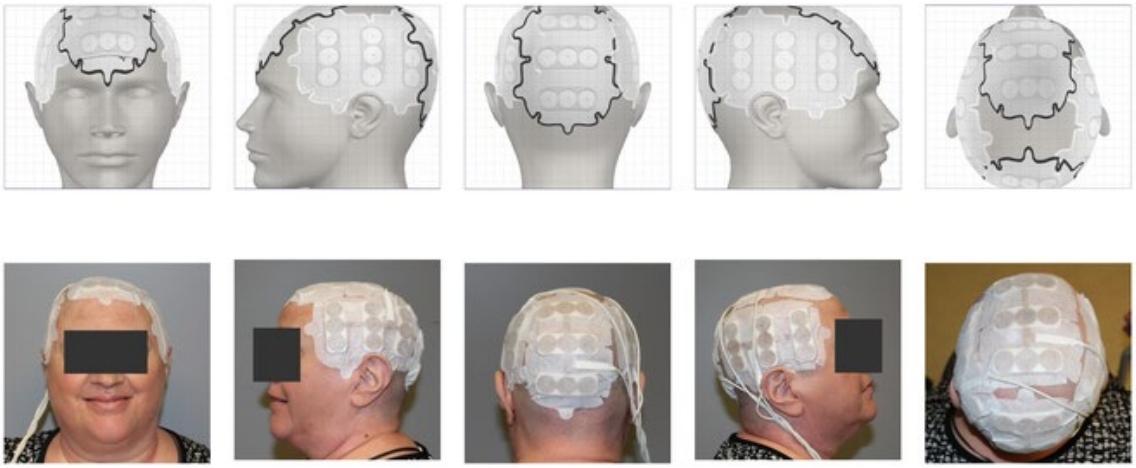

Figure 2: Transducer arrays placement map for GBM treatment using NovoTAL System software.

2.2.5 Mechanism of action of TTFields

The cell cycle of a cell is divided into interphase and mitosis. Interphase is separated into G1, S, and G2, during which cells grow by accumulating biomass through metabolic processes. Mitosis is divided into prometaphase, metaphase, anaphase and telophase, during which biochemical processes predominate to ensure parental genome is sufficiently inherited by newly formed daughter cell. The structural proteins play a key role in these biochemical processes during mitosis and are therefore proposed target of TTFs [76]. Studies have shown that the cells are most vulnerable to TTFs during mitosis part of the cell cycle. During mitosis exposure of cells to TTFs result in violent membrane blebbing and disruption of microtubule spindle elements; chromosomal order is also disrupted in post-mitosis [77, 78]. The fact that TTFields primarily interferes with dividing cells causes the technology to preferentially interact with tissues with a high rate of cell mitosis, such as cancerous tissues, and not affect the normal tissue of the brain.

Proteins possess certain surface charges, depending on the charges of surface amino acids chains. The arrangement of acidic and basic side chains of amino acids can result in regional separation of surface charges and thus creating a dipole moment onto the protein. The dipole moments of such proteins will align within an electric field to orient towards the oppositely charged pole of the filed. The repolarization of the alternating field will lead to re-alignment of the protein dipoles to the opposite pole

within the field. Therefore, such proteins would experience rotational forces within TTFs; this leads to inhibition of protein polymerization and eventually their function [58].

Proteins that are vital for the mitosis and have high dipole moments are likely targets of TTFs, include α/β-Tubulin monomeric subunit of microtubule and the mitotic septin complex. α/β-Tubulin are two heterodimer that are the building blocks of microtubules and possesses a high predicted dipole moment of 1440 Debyes [79]. Studies have shown that TTFs disrupt microtubule polymerization, preventing proper chromosome segregation during mitosis [80]. Therefore, it is possible that TTFs interfere with a critical mitotic function performed by microtubules [58, 59], including the formation of the metaphase and anaphase spindles and their respective mechanical functions [81, 82], or the regulation of cytokinetic cleavage furrow (CCF) that divides the parent cell into two daughter cells [83].

The septin complex consist of 2, 6 and 7 heterodimers and has high dipole moment of 2711 Debyes [78]. It oligomerizes into a highly ordered cytoskeleton-like scaffold that functions to recruit and organize the actinomyosin contractile elements required for the formation of CCF and the separation of the daughter cells [84]. Septins also cross-link F-actin bundles and organize structures such as the cellular sub-membranous actin cytoskeleton [85]. This structure must have adequate rigidity to withstand the hydrostatic pressures generated by ingression of the cytokinetic furrow. Without septin complex, the forces created during cell division can lead to rupture of the plasma membrane, leading to membrane blebbing [86]. Studies have shown that hairpin RNA-driven depletion of septin proteins results in mitotic blebbing with similarities to that seen with TTFs treatment [78].

Unlike errors or damage during the early phases of a cell cycle, errors occurring during late metaphase and in anaphase are unlikely to be corrected [87]. Therefore, TTFs not only cause perturbation of mitosis but also aberrant mitotic exit. This aberrant mitotic exist results in a high degree of cellular stress, as indicated by increased cytoplasmic vacuoles, as well as decrease in proliferation and apoptosis [78]. Cells experiencing mitotic exit in the absence of division have been shown to experience p53-dependent cell cycle arrest and apoptosis [88, 89]. The cells exposed to TTFs exhibit decreased proliferation and increased levels of apoptosis beginning after 24 hours exposure of TTFs in a p53-dependent manner [78].

It has also been suggested that when TTFs are applied to cells during telophase, the hourglass shape of the dividing cells causes the electric fields within the cell to become highly non-uniform with higher field intensities close to the narrow furrow region. Such field inhomogeneity results in dielectrophoretic (DEP) forces. This possibly leading to irregular aggregation of polarizable particles, thereby disrupting cell division [59, 90]. A computational model study that was designed to study the mechanism behind the functioning of TTFields has confirmed this mechanism by showing that the field non-uniformity in dividing cells could eventually cause substantial DEP forces on tubulin dimers and microtubules that can potentially disrupt the cell division [91]. In addition, the study also demonstrated that under the influence of TTFields significant ionic currents could develop along microtubules that can also lead to disruption of the cellular functions [91].

Studies have suggested that TTFs may induce an immunological response against tumors. A study showed that the cells that are experimentally forced to exit mitosis shows the hallmark of immunogenic cell death (ICD) [92]. This immunogenic cell death evokes immune response against the dying cells of the same tumor through expression of cell surface proteins and secretion of cytokines [92-94]. Cells that are expose to the TTFs also express surface proteins such as calreticulin that invoke immunogenic ell death [95]. In clinical setting, the tumor regression is seen in patients with recurrent glioblastoma treated after 6.6-9.9 months [63]. This pattern of delayed response is consistent with an immune mechanism of tumor rejection, and clinical data also suggest that concurrent use of dexamethasone with TTFs is correlated with poor outcome [62, 63]. Recently, studies have also demonstrated that TTFields can inhibit cell migration [96] and DNA damage repair [97, 98].

2.2.6 Factors influencing efficacy of TTFields

The factors that are known to influence the outcome of GBM treatment include: age, KPS, the extent of resection, and morphological, histological and genetic characteristics, such as MGMT tumor mutation status [51, 99]. When treating with TTFields, apart from these known factors, clinical efficacy depends on the level of compliance or device “on-time”, and the distribution and intensity of TTFields in the brain and tumor [61, 100].

2.2.6.1 Compliance

TTFields do not have a systematic half-life like oral or intravenous therapies and exert their therapeutic effect while the electric fields are turned and applied on. Thus, compliance with treatment is critical to maximize effectiveness. Therefore, it is recommended that patient use the Optune device continuously to get maximal benefit. Patient's compliance data is stored on the device, which is available to the physicians. The patients are advised to wear the Optune device for a minimum of 18 hours per day that is equivalent to 75% of compliance. Studies have shown that average monthly compliance rates of 75% improve survival outcomes in recurrent GBM patients compared with lower compliance rates [61, 65]. In newly diagnosed GBM, compliance was shown to be an independent predictor of survival and better outcome with the higher compliance. A threshold value of 50% average monthly compliance with TTFields is required to improve PFS and OS [101]. Patients with a compliance rate of over 90% had a median OS of 24.9 months and a 5-year survival rate of 29.3% [101] .

The patient compliance can be improved by managing the side effects of skin irritation associated with Optune treatment due to transducer arrays [65]. Skin care strategies can help maximize adherence to TTFields treatment while maintaining good quality of life. Prophylactic strategies include proper shaving, cleansing of the scalp, frequent array relocation, use of topical or oral antibiotics, topical corticosteroids, and isolation of affected areas from adhesives and pressure can manage the skin issues [102]. The patience compliance was reported to be also improved with the newer Optune device that is 50% smaller and lighter than the older Optune device that was used during the phase 3 clinical trials [67].

2.2.6.2 Intracranial distribution and intensity of TTFields

The antitumor effect of TTFields is frequency and intensity depended. For glioma cells, maximal inhibition of cellular proliferation was observed at a frequency of 200 kHz, and complete arrest of cellular proliferation occurred when electric field intensity reached 2.25 volts per centimeter (V/cm) [58]. Therefore, intensity of TTFields in the GBM tissue is another important factor that determines the effectiveness of TTFields treatment. TTFields distribution and intensity within the brain, including tumor tissue is influenced by the dielectric properties of different tissue compartments, including skull, scalp, CSF, white and gray matter of brain and tumor tissue [69, 103-105].

2.3 Dielectric properties and intracranial distribution and intensity of TTFields

The electrical properties of a material can be broadly separated into two categories: conducting and insulating. When a conductor is placed in an electric field, free charges move within the conductors until the interior field is zero. On the other side, there are no free charges to move in a dielectric (insulator) in response to an electric field. In polar dielectric such as biological tissue, however, the positive and negative charge centers in the molecules do not coincide and instead exist as dipole. When an electric field is applied to a polar dielectric, it tends to orient the dipoles, which in turn, produces a field inside the dielectric. This internal field inside the dielectric opposes the applied electric field. So, when an electric field, such as TTFields, is applied to a material, the net field (E) inside the material is,

$$E = E_0 - E_p \tag{1}$$

Where, E_0 is the applied electric field and E_p is the electric field produced by the material in response to the applied electric field. Accordingly, the net field is lowered significantly when a material is a dielectric and is essentially zero for a good conductor.

The ability of a material to orient dipoles, also known as polarization, in repose to an electric field is called permittivity and the ability to move charges is called conductivity [106]. The SI units for permittivity is Farad per meter (F/m) and for conductivity is Siemens per meter (S/m). The net field (E) inside a dielectric is define by its permittivity, !!!

$$E = \frac{E_0}{\varepsilon_r} \tag{2}$$

Where, ε_r is the relative permittivity of a material and E_0 is the applied electric field. Therefore, the relationship between permittivity and electric field intensity in a material is inversely proportional.

Conductance is defined as movement of charged particles in a material, which is opposite to resistance to the movement of charged particles in a material. Resistance (R) in a material is given by,

$$R = \rho \frac{l}{A} \tag{3}$$

Where: ρ is the specific resistivity of the material, l is the length of the material, A is the cross-sectional area of the material.

From the equation above, specific resistivity which is an intrinsic property of a material can be given as:

$$\rho = R\frac{A}{l} \tag{4}$$

When an electric field is applied to a material and the flow of charge or current density it produces depends on the specific resistivity of a material. Therefore, the resistivity of a material can be defined as the ratio of the electric field to the density of the current it creates:

$$\rho = \frac{E}{J} \tag{5}$$

Where: E is the electric field intensity, J is the current density. Conductivity (σ) is inverse of specific resistivity (ρ):

$$\sigma = \frac{1}{\rho} = \frac{J}{E}$$

$$\vec{E} = \frac{J}{\sigma} \tag{6}$$

!!! Therefore, the electric field intensity in a material is inversely proportional to its conductivity. However, the higher current induced by the electric field will flow in a material with higher conductivity.

The biological tissue behaves as an inhomogeneous material which displays characteristics of both a dielectric and a conductor because it contain dipoles that can be polarized or rotate as well as has charges that can move in response to an applied electric field [107]. Therefore, conductivity and relative permittivity of a biological tissue determine the electric field intensity in it when an external electric field is applied. In TTFields treatment, the electric field intensity-threshold level of 1-3 V/cm in the GBM tissue is necessary to destroy the tumor cells [59]. Moreover, the dielectric properties of a material depend on the frequency of the applied electric field. Since TTFields are alternating electric field of frequency of 200 kHz, the dielectric properties of different tissue compartments of the brain at this frequency are important to determine the distribution and intensity of TTFields in the brain, including GBM tissue.

The NovoTAL system uses the values of conductivity and permittivity at 200 kHz frequency of various tissue compartments from the literature¸ including scalp [108-111],

skull [112-115], CSF [108, 116, 117], GM and WM [118-123] and GBM tumor [124-127] to predict the best layout plan to place transducer arrays on the scalp so that the GBM tissue receives the therapeutic dose of TTFields. Table 1 shows the values of dielectric properties of various objects and tissue comparts that are used in NovoTAL system to predict the distribution of TTFields within the patient's brain [104].

Dielectric properties	**Scalp**	**Skull**	**CSF**	**GM**	**WM**	**Tumor (core)**	**Gel**	**Transducers**
Conductivity (S/m)	0.25	0.013	1.79	0.25	0.12	0.24 (1.0)	0.10	0
Permittivity (F/m)	10,000	200	110	3000	2000	2000 (110)	100	10,000

Table 1: Values of the dielectric properties of tissues and other material from the literature at 200 kHz

The values of conductivity and permittivity for GBM are derived from four studies: Y Lu et al. measured the dielectric properties of human gliomas at 5-500 MHz [124], Peloso et al. carried out measurement on rat gliomas [125], Surowiec et al. obtained dielectric properties of breast carcinoma [126] and Latikka et al. measured resistivity of human gliomas at 50 kHz. Therefore, there are no values of conductivity and permittivity for GBM at 200 kHz available in the literature. Since the efficacy of TTFields therapy depends on the electric field strength that can be delivered to the tumor; therefore, it is very important to further investigate and determine the dielectric properties of GBM in order to improve outcome of TTFields therapy [105].

The aim of this study was to determine inter-and intra-dielectric properties of GBM tissue to improve the efficacy of TTFields. The other intracranial tumors such as meningioma, low grade glioma, anaplastic glioma and intracranial metastases were also included in this study to compare their dielectric properties with GBM and to get better understanding of the dielectric properties of intracranial tumor tissues at 200 kHz electric field. Moreover, the dielectric properties of a tissue depend on its temperature, and level of water content. This study also focused on examining how temperature, dehy-

dration and irrigation of the tissue can change the dielectric properties of the intracranial tumors in an *in vitro* setting. Histological analysis was also carried out to understand the morphological basis of dielectric properties in GBM tissue.

3. Methods & Materials

3.1 Materials

- 0.9% Nacl solution, Braun, Melsungen, Germany
- 2-Methylbutane, Sigma-Aldrich, Steinheim, Germany
- Ag/AgCl Disc Electrodes (12.5 x 1mm) E204, Warner Instruments, Hamden, U.S.A.
- Application Auto run LCR-GUI-withcancel-Version-V3 and relevant software provided by Novocure, Haifa, Israel
- Bel Premium cotton buds, CMC Consumer Medical Care, Sontheim, Germany
- Cell culture sterile dishes (PS, 100x20 mm), Greiner Bio-One, Frickenhausen, Germany
- Dry Ice, Pharmacy of Universität Klinikum Regensburg
- E4980AL Precision LCR Meter 20 Hz to 1 MHz, BNC-RCA adaptors, test cables and socket clips, reference capacitor, Keysight Technologies, Malaysia
- FileMaker Pro 8.5 Advanced from Claris International Inc., Santa Clara, U.S.A.
- Fine calibrator 530-140, Mitutoya, Japan
- Forceps & Scissor, Fine Science Tools, Heidelberg, Germany
- Forma 900 Series -86 °C Freezer, ThermoFisher Scientific, Czech Republic
- Hera Cell 150 incubator, ThermoFisher Scientific, Langenselbold, Germany
- Hera Safe hood with laminar flow, ThermoFisher Scientific, Langenselbold, Germany
- HISTOSETTE I Tissue processing cassettes, Beloeil, Canada
- Jumper to short LCR meter test cables, Novorcure, Haifa, Israel
- Laptop Thinkpad X240, universal serial bus (USB 2.0) type mini-B, Lenovo, Beijing, China
- Parafilm, American National Can, Chicago, U.S.A.
- Sample holder and Stage, Novocure, Haifa, Israel
- Sample plates, Novocure, Haifa, Israel
- SigmaPlot 13.0, Systal software GmbH, Erkrath, Germany
- Tapira Facial tissues, Friedewald, Germany
- Thermometer, Omega Engineering, INC., Stanford, U.S.A

- Tissue culture plates with six wells,TTP Techno Plastic products AG, Trasaudigen, Switzerland
- Tool Box to short electrodes, Novorcure, Haifa, Israel
- VersaTouch Nitrile gloves, Ansell, Malaysia
- Acetic acid 100%, Merck KGaA, Darmstadt, Germany
- CellSens Dimention 1.18 software, Olympus, Hamburg, Germany
- Coverslips, Carl Roth, Karlsruhe, Germany
- Eosin, Carl Roth, Karlsruhe, Germany
- Ethanol, Sigma-Aldrich, Steinheim, Germany
- Kresyviolett, Sigma-Aldrich, Steinheim, Germany
- Leica CM 1950 cryostat, Leica Biosystems, Nussloch, Germany
- Luxol fast blue, Chroma-Gesellschaft, Münster, Germany
- Meyer's hemalaum solution, Merck KGaA, Darmstadt, Germany
- Microscopic glass slides, Thermo Scientific, USA
- Milli-Q ultrapure water system, Merck Millipore, Darmstadt, Germany
- Neo-Clear, Merck KGaA, Darmstadt, Germany
- Neo-Mount, Merck KGaA, Darmstadt, Germany
- Olympus BX51 microscope, Olympus, Hamburg, Germany
- Olympus IX7O microscope, Olympus, Hamburg, Germany
- Olympus XC10 camera, Olympus, Hamburg, Germany
- Paraformadlehyde 95%, Sigma-Aldrich, Steinheim, Germany
- Staining chamber of Hellendahl, Carl Roth, Karlsruhe, Germany
- Tissue-Tek, Sakura Finetek Europe. B.V, Alphen, Netherland
- Xylol 98%, Carl Roth, Karlsruhe, Germany

3.2 Methods

To determine the conductivity and permittivity of intracranial tumor tissues, impedance was measured. Electrical impedance is the measure of the opposition that a circuit presents to a current when an alternating voltage is applied such as in TTFields, and it has SI unit of ohm (Ω). Impedance consist of two components: real component and imaginary component. Real component is pure resistance of the system, which is directly related to the conductivity or resistivity of a material. Imaginary component of impedance further has two parts: inductive reactance and capacitive reactance [128].

Inductive reactance is the resistance that current faces due to the magnetic field produced by the alternating flowing current. This is related to the conductivity of a material. Capacitive reactance is the resistance that current encounters from the intrinsic current created by the electrostatic storage of charges. A dielectric material has the ability to store charges, which is also called capacitance and it is related to its permittivity. Impedance is a complex number which defined by magnitude and a phase factor. The magnitude of impedance act like real or resistive component that gives the drop in voltage amplitude, while phase factor ($\angle\theta$) of impedance shows that the current lags the voltage by a phase or an angel [128]. Total impedance can be written as:

$$\mathrm{Z} = \mathrm{Zre} + \mathrm{Zim} \tag{7}$$

Where: Z is the total impedance, Zre is the real or resistive component and Zim is the imaginary or reactive component. Therefore, it is important to measure the impedance of the tissue in order to determine its conductivity and permittivity when alternating voltage is applied.

In this study, impedance of intracranial tumor tissues was measured at 200 kHz electric field because the maximal inhibition of tumor cell division in GBM by TTFields was induced at a frequency of 200 kHz. It was measured *in vitro* by utilizing the parallel-plates method, Ag/AgCl disc electrodes (12.5 x 1mm) that reduce electrode-polarization at this frequency, and the E4980AL Precision LCR meter (impedance analyzer) with the systematic error of 0.05%. The LCR meter measured the Zre and Zim of the tumor tissues. These values were used to solve the parallel-plates method equations

$$\sigma = \frac{\mathrm{d} \cdot \mathrm{Zre}}{\mathrm{A}(\mathrm{Zre}^2 + \mathrm{Zim}^2)} \qquad \varepsilon_\mathrm{r} = \frac{\mathrm{d} \cdot \mathrm{Zim}}{\mathrm{A}\omega(\mathrm{Zre}^2 + \mathrm{Zim}^2)} \times \frac{1}{\varepsilon_0} \tag{8),(9}$$

Where,

$\sigma = \text{conductivity (Siemens/m)}$

$\mathrm{A} = \text{tissue cross section area } (\mathrm{m}^2)$

$\mathrm{d} = \text{tissue thickness (m)}$

$\mathrm{Zre} = \text{real component of impedance } (|\mathrm{Z}| \cos\theta)$

$\mathrm{Zim} = \text{imaginary component of impedance } (|\mathrm{Z}| \sin\theta)$

$\varepsilon_\mathrm{r} = \text{relative permitivity (Farad/m)}$

$\varepsilon_0 = \text{vacuum permitivity (F/m)}$

$\omega = 2\pi\mathrm{f} = 2 \text{ x } 3.14 \text{ x } 200 \text{ KHz}$

to obtain the conductivity and relative permittivity of the tumor tissues. The equations are given below,

The tumor tissues for measurements were obtained from the patients who had only tumor pathology and went under surgical resection between 09/2018-07/2020 at the neurosurgery department of the University Hospital of Regensburg. The study was approved by the ethical committee of the University Hospital of Regensburg (18-884-101). There was no external financial support for this study.

3.2.1 Measurement equipment setup

The measurement system to calculate the impedance of the tumor tissues is demonstrated in Figure 3.

1. LCR meter+ BNC-RCA adoptors
2. LCR-test cables with output sockets
3. Jumper to short LCR test cables
4. Stage and sample holder
5. Application LCR-GUI
6. Tissue sample
7. Tissue sample plates
8. Box to short electrodes
9. Ag/AgCl electrodes

Figure 3: Overview of equipment used to measure impedance of the tumor tissues

The components of the measurements system are described in detail below,

- E4980AL Precision LCR meter: The BNC-RCA adaptors and coaxial test cables were connected to the measurement output terminal of the LCR meter accord-

ing to the 4-Terminal scheme described in the Impedance Measurement Handbook (Keysight, 6th addition). This configuration allows to measure impedance in the range of 10mΩ -10kΩ. The socket clips were attached at the end of the test cables to connect the electrodes pins. The LCR meter was supplied with the alternating current through its power cable. After connecting the BNC-RCA adopters and electrical cables, the accuracy of the LCR meter was verified by using a reference capacitor with a known capacitance. It is very important to connect the BNC-RCA adopters and electrical wires properly as it can affect the accuracy of measurements. The LCR meter should be turned on at least 30 minutes before the measurements according to the manufacture instructions.

- Jumper to short LCR meter test cables: The short measurements were performed before the measurements to determine the internal impedance of the system. For this purpose, a jumper was used to short the LCR meter teste cables (Figure 4). When the internal impedance of the system is of the same order of magnitude as the tissue sample impedance, then it should be subtracted from the measurements. If the internal impedance is very small than the measured impedance, then it can be ignored. In our measurements the internal impedance was very small as compared to the measured impedance and therefore was neglected.

Figure 4: Short measurement of the LCR meter.

- Ag/AgCl disc electrodes (12.5 x 1mm): The Ag/AgCl electrodes were attached to the wires extension with pin clips at the end for connection with the LCR meter output. After their usage, they were cleaned with saline solution by using cotton buds. They were stored before and after their use in a darker place to avoid discoloration due to exposure to light, although it does not impair their function. However, the electrodes were replaced with new ones when their surface became glossy and scratched after a lot of measurements.

- Tool box to short electrodes: The Ag/AgCl electrodes were shortened by placing their pin clips in a specially designed tool box (Figure 5). The pre-conditioning of the electrodes before the measurements was done by covering their whole surface in 0.9% NaCl solution. Two pairs of electrodes were prepared in event of breakage of an electrode during the measurement, extra electrode was available to use immediately.

Figure 5: Electrodes conditioning: electrodes were short using a tool box and placed in saline solution for at least 30-60 minutes before measurements

- LCR-GUI V.3 application: The LCR meter operation was controlled through the LCR-GUI application installed in the laptop. This application also allowed to save the LCR measurements automatically in excel files. The laptop and the LCR meter were connected with each other through a universal serial bus (USB 2.0) type mini-B cable.
- Stage and sample holder: A specially designed stage and holder was utilized to hold the sample plate and electrodes in a stable position to avoid any movement during the measurements (Figure 6).

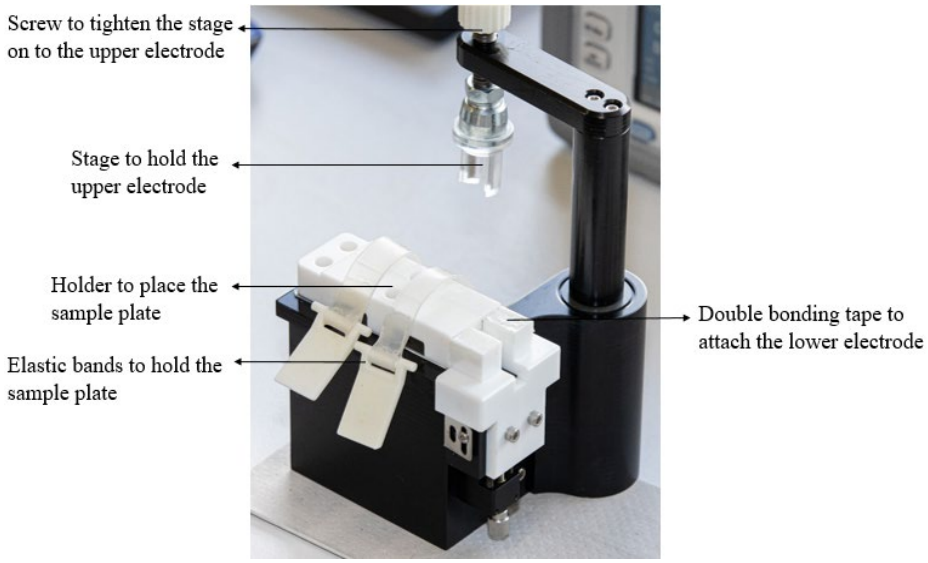

Figure 6: Specially designed stage and sample holder

- Sample plates: The specially designed sample plates had cylindrical holes in them were the sample tissue was placed for measurements. The diameter and

length of these cylindrical holes represented the area and length of the sample tissue respectively (Figure 7).

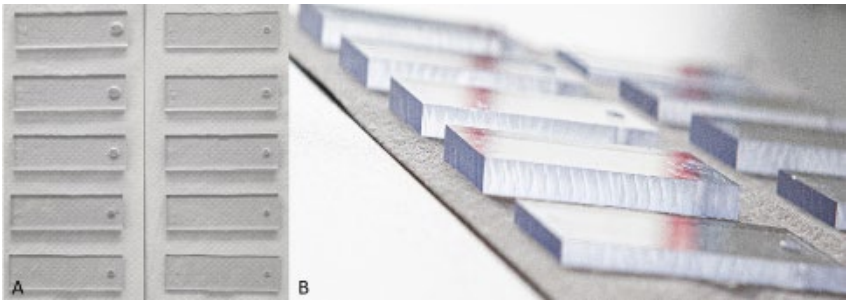

Figure 7: Samples plates with cylindrical holes of various diameters (photo A) and thickness (photo B)

3.2.2 Collection of tumor tissue samples and pre-measurement preparations

A fast acquisition protocol was followed to collect the tumor tissue from the operation room and then measuring its impedance in a laboratory setting. The pre-measurement preparations were also carried out during the fast acquisition protocol. The fast accusation protocol and pre-measurement preparations are explained below,

- Planning with surgeon: When a tumor-resection was scheduled in the OP-Plan, the surgeon was contacted pre-operation to discuss the availability of the post-resection tumor tissue for the impedance measurements.
- Pre-measurement preparation: After confirmation of the tumor tissue availability by the surgeon, the pre-measurement preparation was carried out at least one hour before the resection of the tumor. The LCR-meter and the laptop were turned on and connected through LCR-GUI application. The Ag/AgCl electrodes were conditioned in 0.9% NaCl solution. Cell culture plates were placed in the Hera Cell 150 incubator to warm up the tumor tissue. For drying out the tumor tissue, cell culture plates were placed in the Hera Safe hood with turned on laminar flow. 0.9% NaCl solution was put in cell culture plates to irrigate the tumor tissue.
- Communication between operation room and lab: The laboratory received a call to collect the tumor tissue from the operation room at least 15-20 minutes before the tumor tissue resection.
- Collection of the tumor tissue from operation room: The tumor tissue was collected from the operation room right after its resection from the patient. The tissue was collected in the sterile 6-well tissue culture plate, without any liquid,

that was then sealed with the parafilm and covered by the latex gloves to avoid dehydration. The patient information was also taken from the operation room.

- Transport of tumor tissue to laboratory: The tissue sample was transported in a safe foam box to the laboratory. It took 10-15 minutes to reach the laboratory from the operation room.

3.2.3 Impedance measurements of the tumor tissue

Then measurements were immediately carried out upon arrival in the laboratory by following the steps described below in order,

- The patient code was given in the LCR-GUI application.
- Short measurement was performed as shown in figure 4.
- A pair of conditioned electrodes (Figure 5) was taken out of saline solution and dried well with cotton buds. Electrodes were connected to the LCR meter test cables and the lower electrode was attached to the holder (Figure 9).
- Tumor tissue was placed in holes of the sample plates gently using a fine tweezer to avoid any distortion of tissue structure. Tumor tissue was placed in such a way that only 0.5mm to 1.5 mm of it stood out of the holes. (Figure 8)

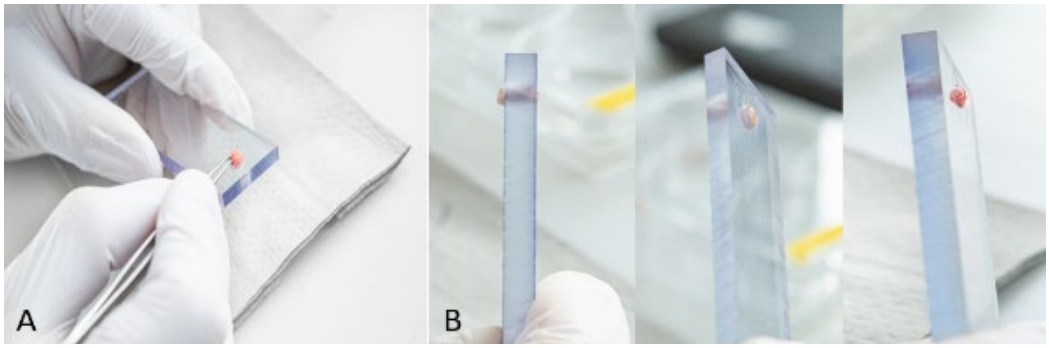

Figure 8: A) careful placement of the tumor tissue into the sample plates holes. B) 0.5 mm to 1.5 mm of the sample tissue stood out from the sample plate

- The thickness and diameter of the holes were noted that corresponded to the size of the tumor tissue in them.
- The sample plate containing the tissue was placed on the holder while ensuring a perfect contact between the tissue sample and the lower electrode. The sample plate was strapped tightly with the elastic bands. (Figure 9)
- The upper electrode was placed gently on the tissue sample, and tighten at a stable position with the stage by turning the screw clockwise. (Figure 9)
- Subsequently, the measurement was run using the LCR-GUI application.

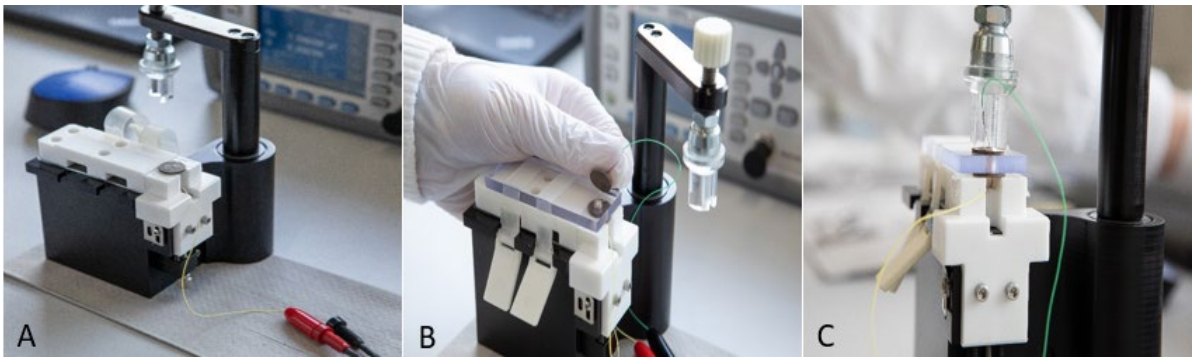

Figure 9: Electrodes and tissue sample plate set-up. A) Lower electrode attached to the holder. B) Sample plate and upper electrode placement on the holder. C) The sample plate and electrodes are held in stable position with the holder and the stage. It is very crucial to have a perfect contact between the two electrodes and the tissue sample

3.2.4 Effect of temperature, dehydration and irrigation on impedance

The temperature difference between the room and the body could influence the impedance. The measurements were performed after around 15 minutes of tissue extraction, which could lead to dehydration of the tumor tissue before the impedance measurements. Further, the tumor tissue was irrigated with saline solution by the surgeon before extraction and this could also affect the impedance. Therefore, these artifact conditions were created in the laboratory setting to determine the effect of temperature, dehydration and irrigation with NaCl 0.9% solution on the impedance measurements (Figure 10). The impedance measurements were carried out first under normal conditions and then after the artifact conditions to make a comparison.

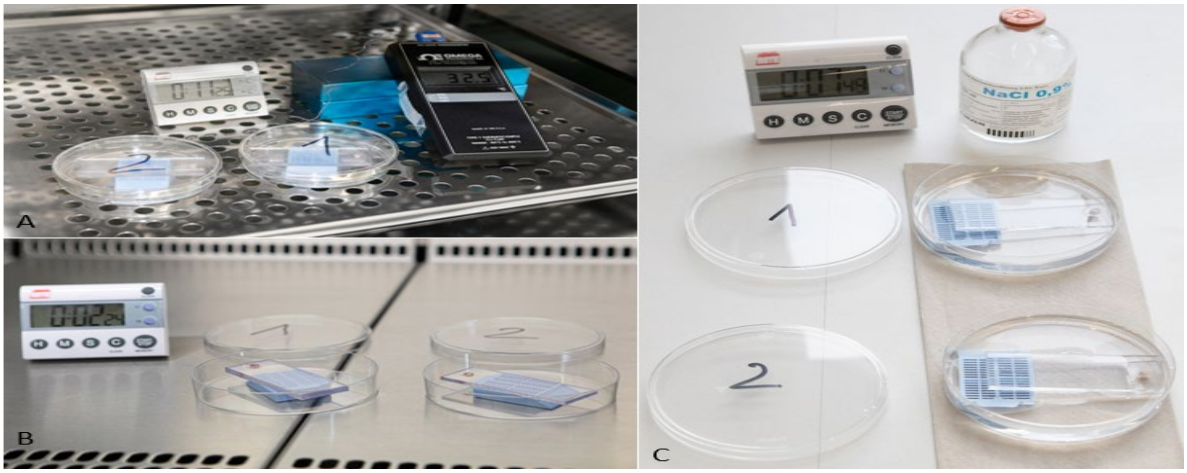

Figure 10: Experimental artifacts conditions. A) The tissue sample was placed in the incubator for 60 minutes to achieve 35°C B) The tissue sample was dehydrated in the hood with laminar flow for 15-30 minutes C) The tissue sample was irrigated in saline solution for 5-10 minutes.

The tumor tissues were frozen immediately after the measurements by using 2-methybutane and placed in dry ice. The tissue samples from each patient were assigned to a biobank number and stored in Forma 900 freezer at -80 °C.

3.2.5 Histological analysis of GBM tissue

The histological analysis of the GBM tissue, previously frozen at -80 °C after impedance measurements, was performed. The GBM tissue samples were stained with Hematoxylin and Eosin (H&E) and Luxol Fast Blue (LFB) according to the methods described by P. Böck [129]. Before the staining, the GBM tissue was cut into 10 µm cryosections by using the Leica CM 1950 cryostat and Tissue-Tek was utilized as embedding medium to avoid movement of the tissue during the cutting process. The cryosections were then frozen at -80 °C until the staining process. The H&E stain was used to stain the nuclei of the cells as blue and cytoplasm and extracellular matrix as red-pink, and LFB was used to stain the myelin as blue.

For H&E staining, the tissue cryosections were placed on microscopic glass slides to thaw and dry at room temperature. Then stained with Mayer's hematoxylin for 5 minutes in the staining chamber of Hellendahl. The tissue was rinsed within the staining chamber with running tap water for 10 minutes. Eosin staining was done by dipping the tissue in 0.5% water dissolved Eosin. The tissue was then rinsed in demineralized water until the eosin stopped streaking. To remove the water from the tissue, it was treated with increasing concentration of ethanol. At first the tissue was swirled with 70% ethanol carefully to ensure the differentiation of the tissue is not affected. Then the tissue was rinsed in 96% ethanol for 1-2 minutes and then 2x1-2 minutes in 100% ethanol. In the end, the tissue was rinsed with Neo-Clear three times for 10-20 minutes and covered waterless with coverslip using the Neo-Mount.

For LFB staining, the tissue cryosections on microscopic glass slides were thawed and dried at room temperature and then fixed in 4% paraformaldehyde for 10 minutes. The tissue was washed with distilled water three times for 5 minutes. Then tissue was incubated with 0.1% luxol fast blue (0.1g luxol fast blue in 100 ml 95% ethanol + 0.5 ml 10% acetic acid) in the staining chamber of Hellendahl at room temperature for 24 hours. After the incubation, the tissue was first washed with 95% ethanol and then thoroughly with distilled water. For differentiation, the tissue was dipped in 0.05% lithium carbonate solution (0.05g in 100 ml distilled water) for 30 second. The tissue was

rinsed in 70 % ethanol for further differentiation. Then the glass slides were placed in distilled water and microscopic control with Olympus IX70 was made to monitor the differentiation process. After ensuring good differentiation of the tissue, the tissue was incubated with 0.1% crystal violet (0.1g crystal violet in 100 ml distilled water) for 50-60 seconds. Then the tissue was washed in distilled water to remove the extra stain. To remove the water from the tissue, the tissue was first rinsed for 5 minutes in 96% ethanol. Then dipped in 100% ethanol two time for 10 minutes each and then also 2x10 minutes in xylol. The tissue was covered with coverslips by using the Neo-Mount.

The stained GBM tissues were analyzed with the Olympus BX51 microscope and images were taken using the Olympus XC10 camera. The images were processed in the CellSens Dimensions 1.18 software and saved as TIFF files.

3.2.6 Statistical analysis of the data

The calculations of conductivity and permittivity from impedance values were carried out with Microsoft Excel 2016. The calculations for statistical analysis along with statistical tests were performed with Stata/IC 16.1 (Stata Corporation, College Station, USA) and a p value ≤ 0.05 was rated as statistically significant. The diagrams were generated with SigmaPlot 13.0. Only meningiomas, low grade gliomas, anaplastic glioma, GBM and metastasis were included in the statistical analysis, while other tumor entities were left out due to low set of measurements. GBM and anaplastic gliomas were combined together as one histological entity under high grade gliomas for statistical analysis purposes.

The main focus was to determine if the dielectric properties of each tumor entity was significantly different from each other and for this purpose one-way analysis of variance (one-way ANOVA) and a multiple comparison test (Holm-Sidak method) were performed. A 2-sample t-test was carried out to conclude if there was a difference between the dielectric properties of solid and necrotic part of the GBM. To establish the effect of artifacts (temperature, drying and irrigation) on measurements of dielectric properties, a preliminary normality test (Shapiro-Wilk) for the normal distribution of population was conducted and based on its result a nonparametric test (Mann-Whitney Rank Sum test) was performed.

The mean values of dielectric properties of each histological group were descriptively evaluated along with their respective standard deviation and standard error. Further,

the results were analyzed through column chats demonstrating mean values, measurement ranges and 95% confidence interval bars. The dielectric properties of each GBM case were also analyzed by plotting their minimum, maximum and mean values in dot plots.

4. Results

4.1 Demographics of study population

The study population in this study consisted of 130 patients who underwent surgical resection to remove intracranial tumors and metastases. The age of 130 patients at the time of surgical resection ranged between 10.5-84.8 years with an average age of 59.3 years. The 55.38% of study population consisted of females and 44.62% of male. The main diagnosis was GBM (30%), meningioma (27.6%), metastases (22.31%), anaplastic gliomas (9.23%), low grade gliomas (5.38%) and other types of tumors such as neuroma, craniopharyngioma (3.08%). The other types of tumors were not included in the statistical analysis of this study due to insufficient measurements. The demographic data of the study population in this study is presented in Table. 2.

Parameter	
Total Number	130
Gender	
• Female	72 (55.38%)
• Male	58 (44.62%)
Age (mean)	59.3 (range: 10.5 – 84.8)
Diagnosis	
• GBM	39 (30%)
• Meningioma	36 (27.6%)
• Metastases	29 (22.3%)
• Anaplastic glioma (WHO grade 3)	12 (9.23%)
• Low grade glioma (WHO grade 2)	7 (5.38%)
• Other (Neuroma, craniopharyngioma)	4 (3.08%)
• Tumor free	3 (2.31%)
MGMT promoter status (GBM)	
• Methylated	20 (51.28%)
• Unmethylated	19 (48.72%)
MGMT promoter status (All Gliomas)	
• Methylated	33 (56.90%)
• Unmethylated	25 (43.10%)

Table 2: The demographics of study population: Patients with brain tumors, treated with surgical resection between 09/2018-07/2020

Molecular characterization of the gliomas was also performed in this study, and the MGMT promoter status was approximately equally distributed in GBM patients; where

51.28% had methylated MGMT promoter and 48.72% had unmethylated MGMT promoter. When all types of gliomas were combined together as one histological entity then 56.90% of all gliomas had methylated MGMT promoter and 43.10% had unmethylated MGMT promoter.

4.2 Conductivity of intracranial tumors and metastases

The highest number of impedance measurements in this study were performed with tumor tissue from gliomas followed by meningioma and then brain metastases. The results of impedance measurements showed that the mean values of conductivity were statistically different for each histological entity, but at the same time wide range of variation in conductivity values also existed within and between each tumor tissue type. The conductivity of gliomas was the highest among the other types of brain tumor tissue, including meningioma and metastasis. Although the conductivity of high grade gliomas was higher than low grade glioma, this was not statistically different. The meningiomas showed the lowest conductivity among the intracranial tumors. The descriptive numbers of conductivity for each histological entity are given in Table 3, and statistical comparison is shown in Figure 11.

Parameter				
Diagnosis	**Number of measurements**	**Conductivity (S/m)**	**Standard deviation (STD)**	**Standard error (SE)**
Meningioma	143	0.203	0.075	0.00633
Metastasis	112	0.317	0.109	0.0103
Low grade glioma	28	0.325	0.171	0.0322
GBM	204	0.353	0.133	0.00929
		P = < 0.001		

Table 3: Descriptive results: conductivity of intracranial tumors and metastasis at 200 kHz electric field, at room temperature

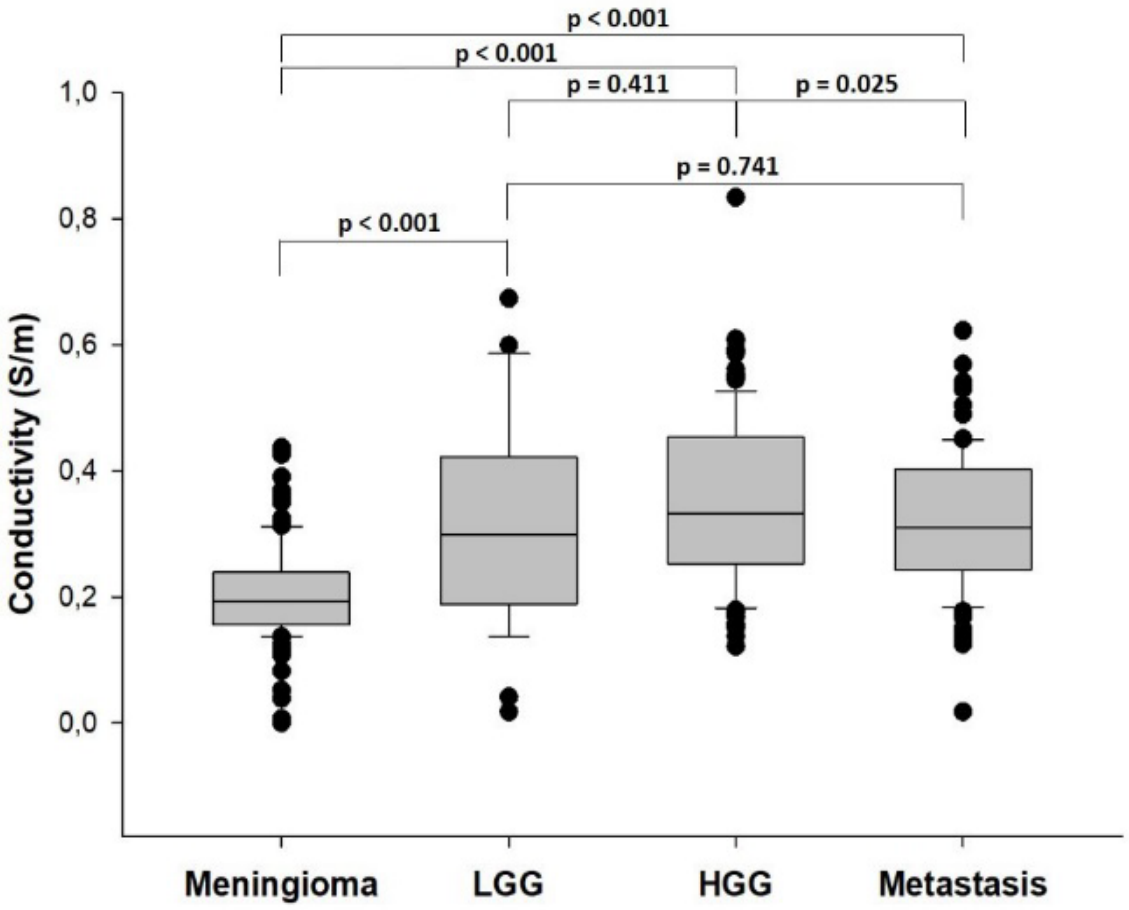

Figure 11: Statistical comparison of conductivity of intracranial tumors and metastasis at 200 kHz electric field, at room temperature.

4.2.1 Conductivity of GBM

In total 204 impedance measurements were performed on malignant glioma tissue obtained from 54 patients. The measurements were carried out with the tissue from different parts of the same tumor, including solid and necrotic part. The results showed that the mean conductivity value of malignant glioma was 0.353 S/m with SD of 0.133 and. However, there was a considerable variability in conductivity values of GBM tissue, not only between individual patients but also within the same patient. The conductivity values for each GBM patient of solid compartment is demonstrated in Figure 12. Within the GBM tumor, the conductivity of the solid part was 0.369 S/m and of the necrotic part was 0.260 S/m, which was statistically significant (p = 0.0008). Leven's test (p=0.004) showed that the variability of the conductivity values was significantly

different between the solid and perinecrotic compartment. The variability of conductivity was higher in the solid compartment compared to the perinecrotic area. Figure 13 presents the comparison of conductivity between solid and necrotic part of the GBM.

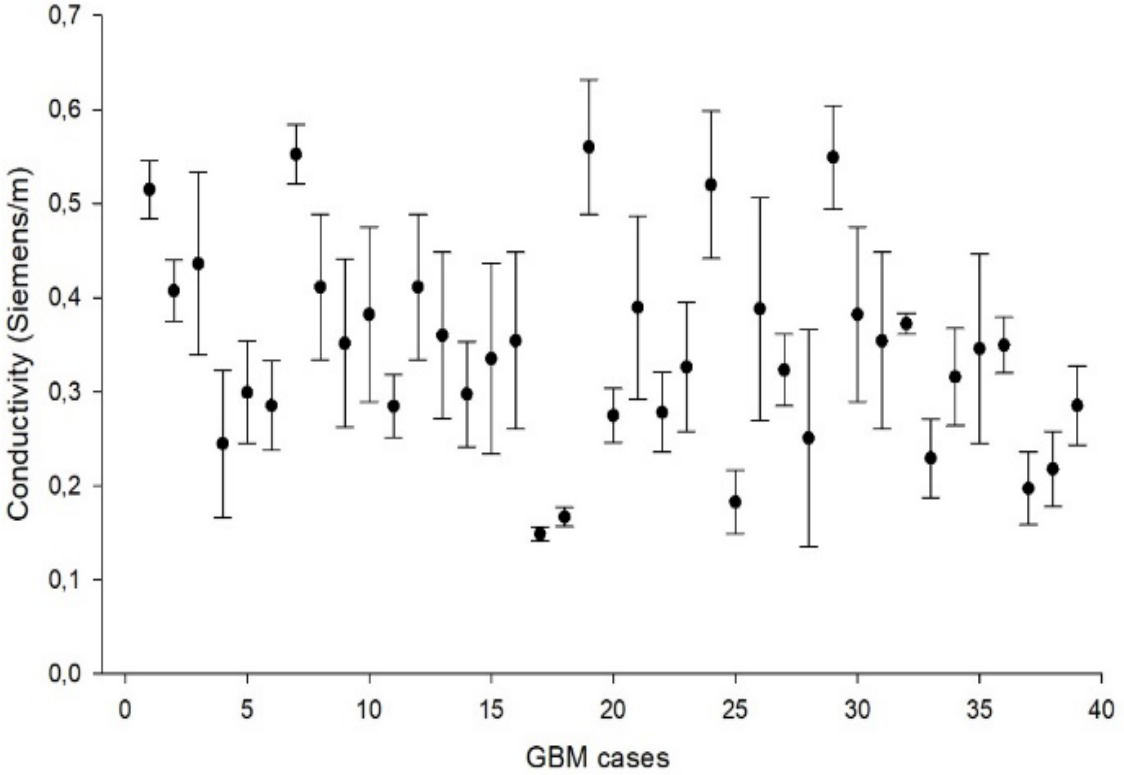

Figure 12: Average, minimum and maximum tumor conductivity at 200 kHz electric field for each patient of solid compartment showing high inter- and intra-individual variability.

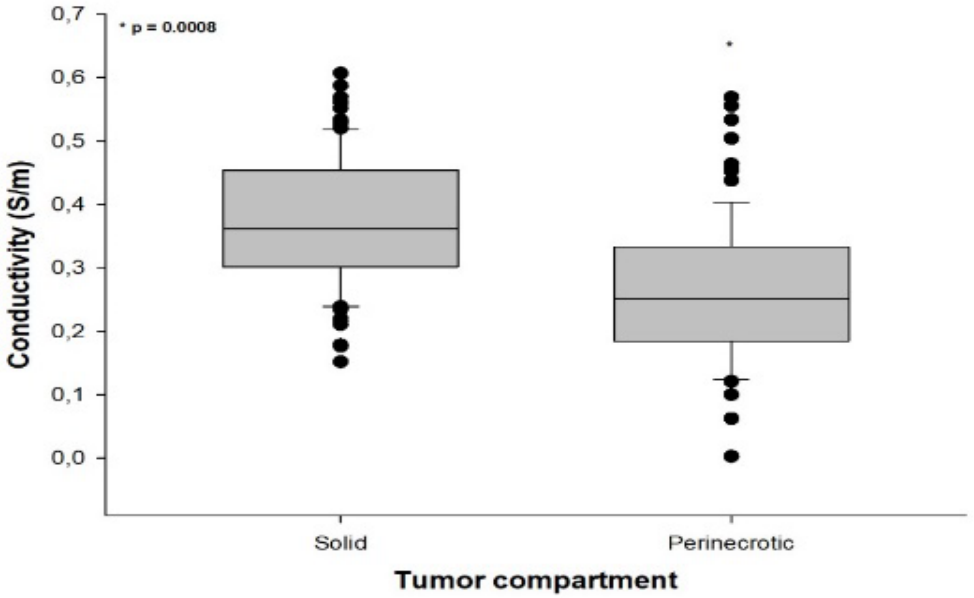

Figure 13: Conductivity comparison of solid and perinecrotic parts of GBM at 200 kHz electric fields

4.2.2 The effect of artifacts on conductivity

There was no statistical difference in conductivity values of intracranial tumor tissue at room temperature and at 35 °C (Figure 14). On the other side, the conductivity of the tumor tissue decreased significantly after drying and increased statistically after irrigation with 0.9% NaCl saline solution (Figure 15 & 16).

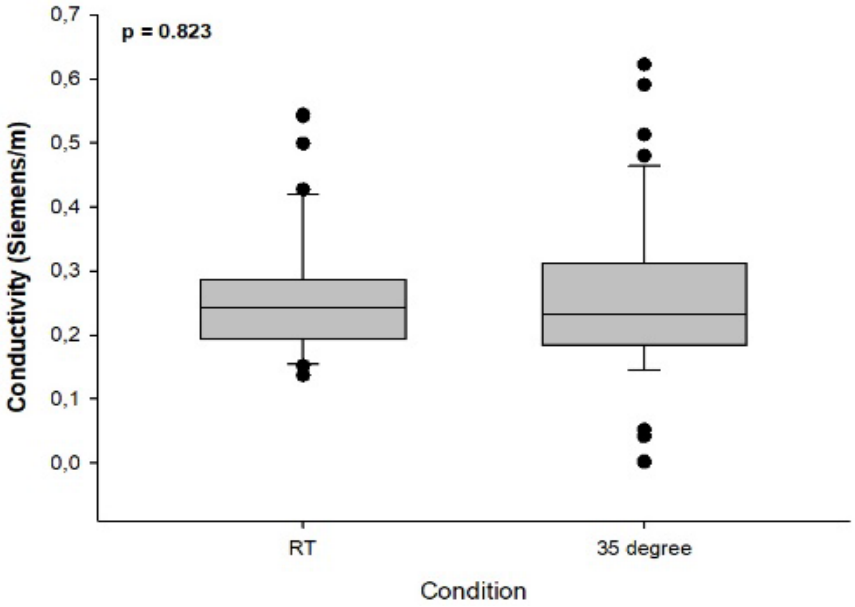

Figure 14: Conductivity of intracranial tumors at 200 kHz electric field under room temperature (RT) and at 35 °C.

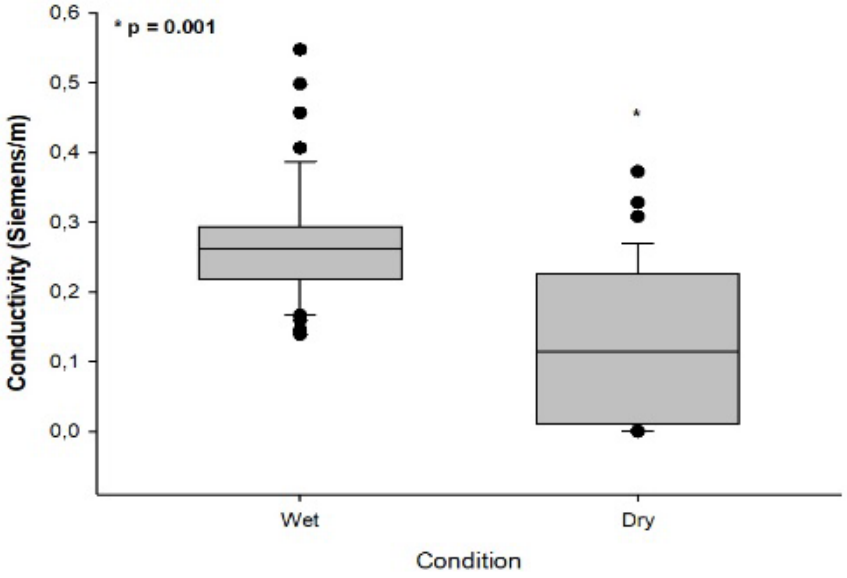

Figure 15: Conductivity of intracranial tumors at 200 kHz electric field measured with post-excised tissue (wet) and drying the tissue for 15-30 minutes under the laminar flow hood.

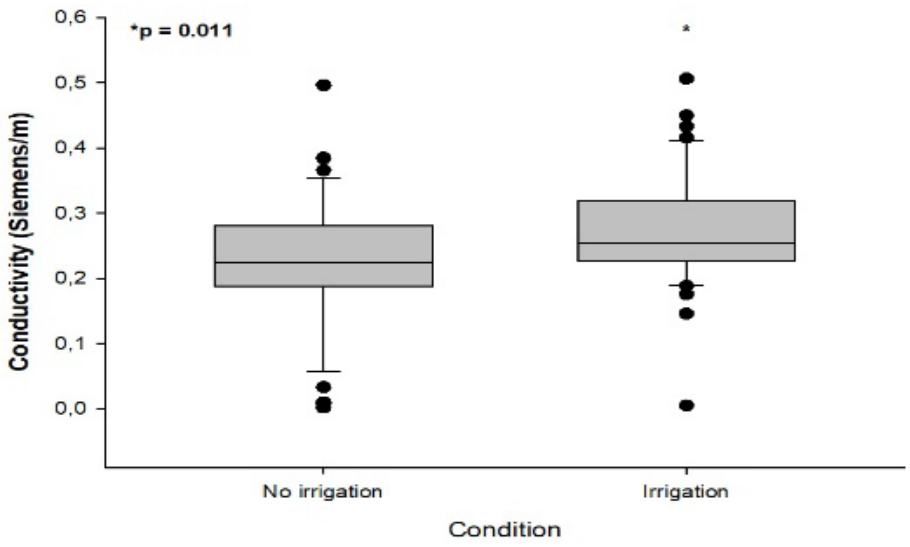

Figure 16: Conductivity of intracranial tumors at 200 kHz electric field with post-excised tissue (no irrigation) and irrigation with 0.9% NaCl saline solution for 5-10 minutes

4.3 Permittivity of intracranial tumors

The statistical difference existed in the mean values of permittivity for each histological group, but we also observed a high degree of variability within the data. The meningioma showed the highest permittivity in this study followed by metastasis, GBM and then low grade glioma. The low grade glioma exhibited significantly lower permittivity than high grade glioma, metastasis and meningioma. There was no pattern observed in permittivity among intracranial tumors as compared to the conductivity where the values increased as the tumor tissue was more malignant. The descriptive values of permittivity for each histological group are given in Table 4 and statistical comparison is presented in Figure 17.

Parameter				
Diagnosis	**Number of measure-ments**	**Permittivity (Farad/m)**	**Standard de-viation (STD)**	**Standard error (SE)**
Meningioma	143	4331.536	1480.247	123.784
Metastasis	112	4245.766	1805.101	170.566
Low grade glioma	28	2538.122	1574.297	297.514
GMB	204	3896.778	2461.872	172.366
		P = < 0.001		

Table 4: Descriptive results: permittivity of intracranial tumors and metastasis at 200 kHz electric field, at room temperature

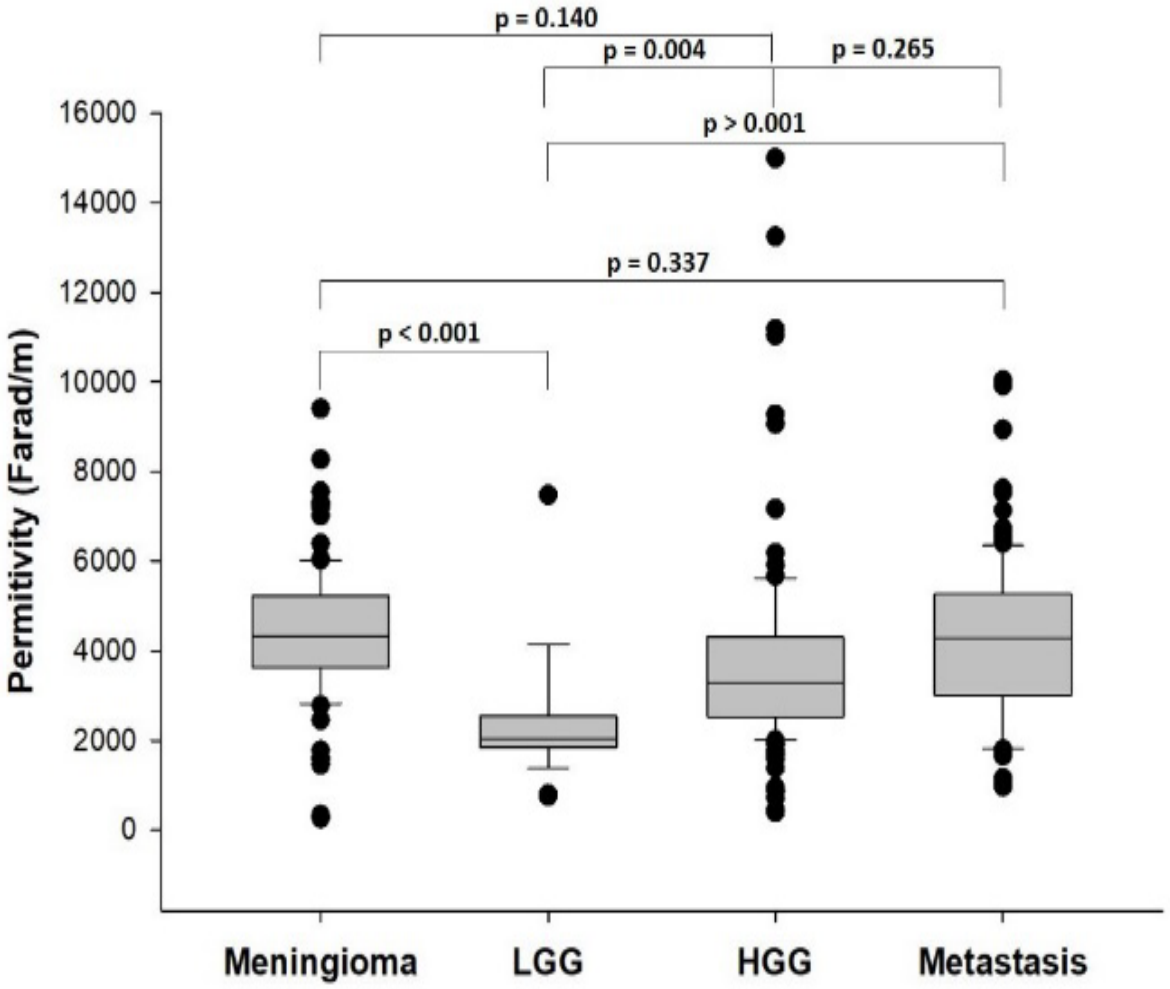

Figure 17: Statistical comparison of permittivity of intracranial tumors and metastasis at 200 kHz electric field, at room temperature.

4.3.1 Permittivity of GBM

This study showed that the mean permittivity value of GBM was 3896. 778 Farad/m, which was higher than low grade gliomas but lower than other brain tumor tissue. However, similar to the conductivity of GBM, great range of variation existed between individual patients and also within the same patient (Figure 18). Comparing the permittivity of different parts of the GBM, the permittivity of the solid part was 4382.589 Farad/m and of the necrotic part was 2916.875 Farad/m. The standard deviation and standard error for the solid part of the tumor was higher than the necrotic part. Leven's test (p=0.00001) showed that the variability of the permittivity was significantly different between the solid and perinecrotic compartment. The permittivity showed higher variation in solid part as compared to the necrotic part of the tumor. Further, the necrotic

part of the GBM exhibited significantly lower permittivity as compared to the solid part (Figure 19).

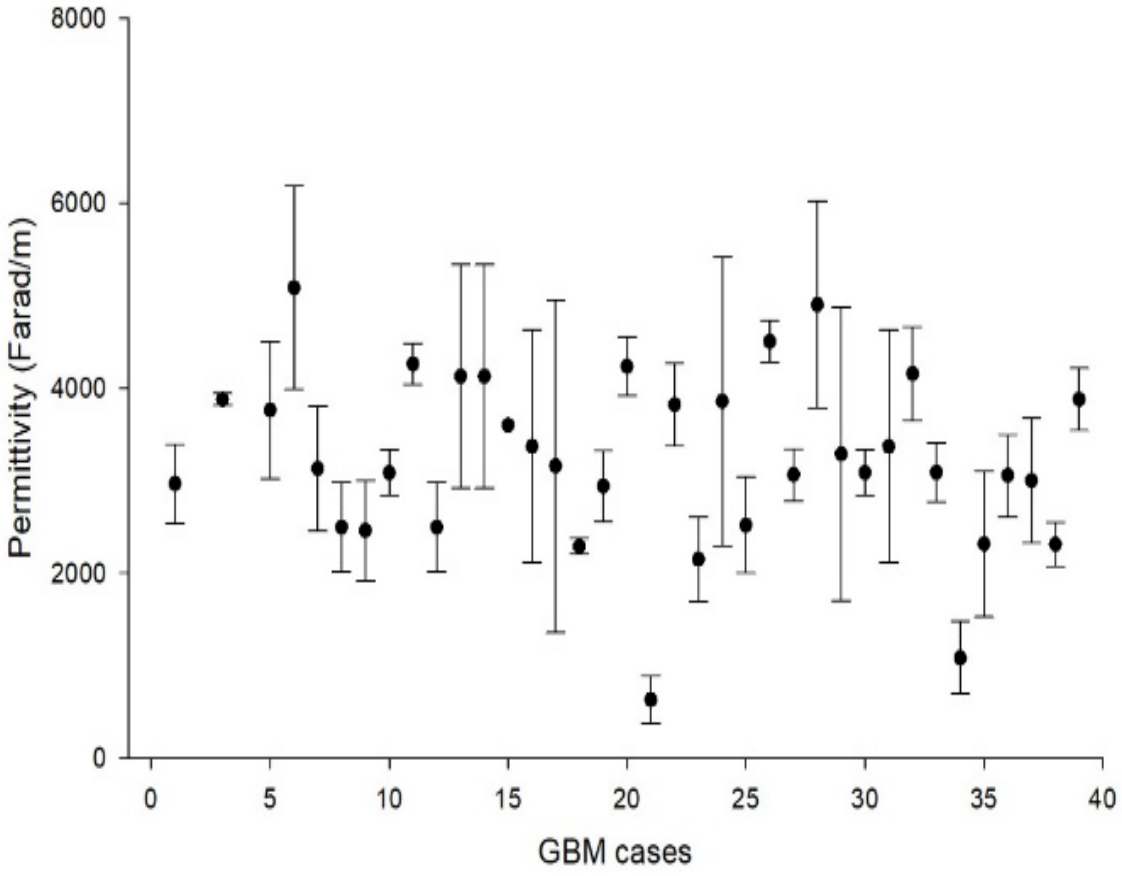

Figure 18: Average, minimum and maximum GBM permittivity at 200 kHz electric field for each patient showing high inter- and intra-individual variability.

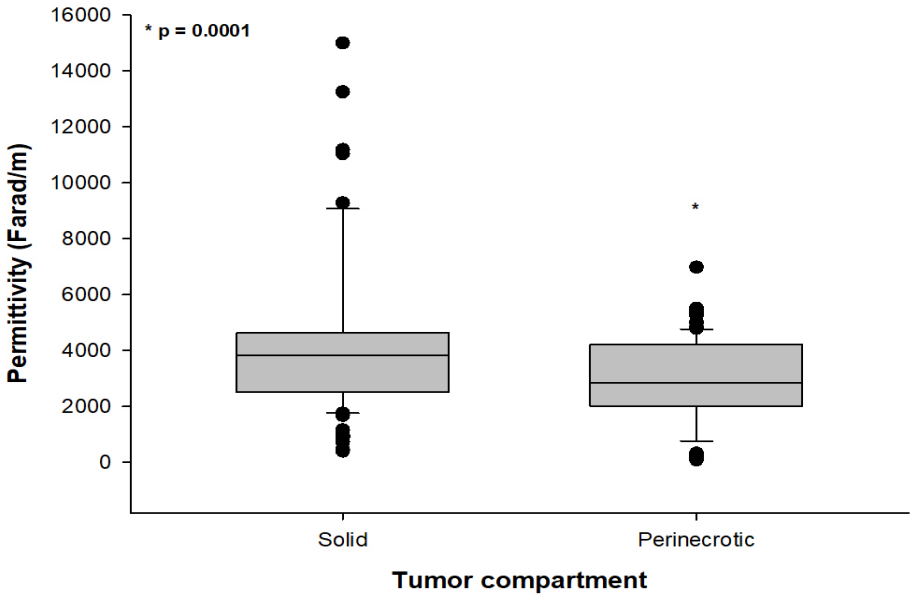

Figure 19: Difference in permittivity of solid and perinecrotic parts of GBM at 200 kHz electric field

4.3.2 The effect of artifacts on permittivity

There was no statistical difference in permittivity of intracranial tumors at room temperature and at 35 °C (Figure 20). The permittivity of the tumor tissue decreased significantly after drying of the tissue (Figure 21). Further, irrigating the tumor tissue with 0.9% NaCl saline solution had no statistically significant effect on the permittivity measurements (Figure 22).

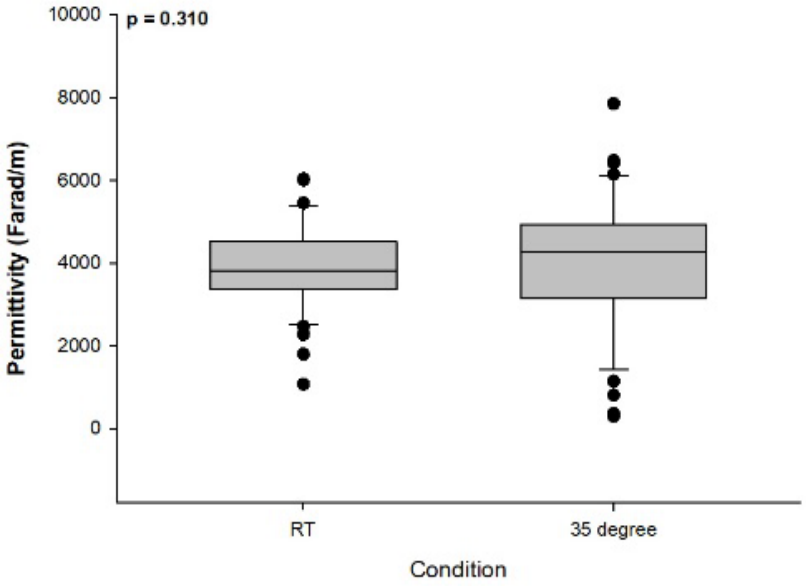

Figure 20: Permittivity of intracranial tumors at 200 kHz electric field under room temperature (RT) and heating up the tissue for 60 minutes in the cell incubator to achieve 35 °C.

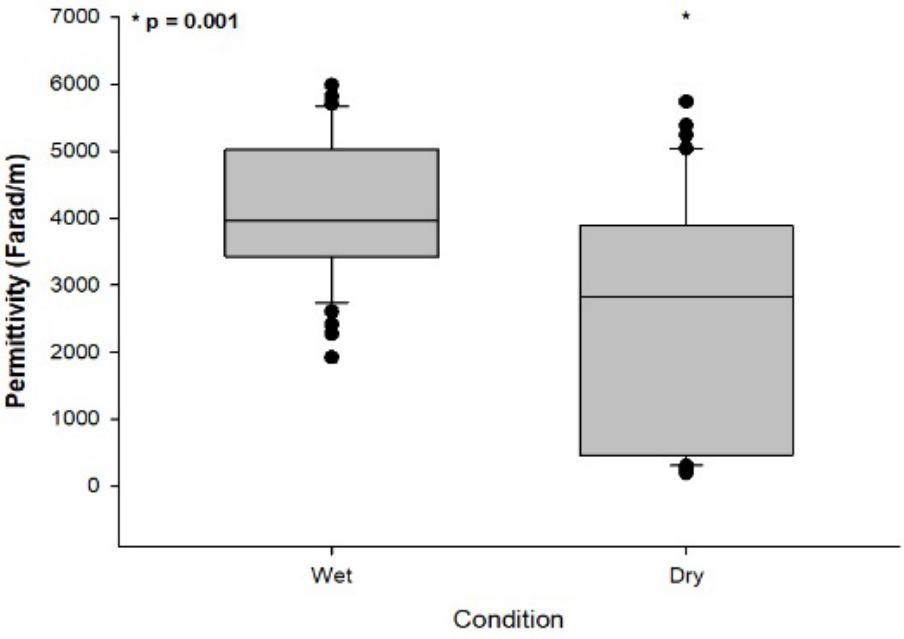

Figure 21: Permittivity of intracranial tumors at 200 kHz electric field measured from post-excised tissue (wet) and drying the tissue for 15-30 minutes under the laminar flow hood.

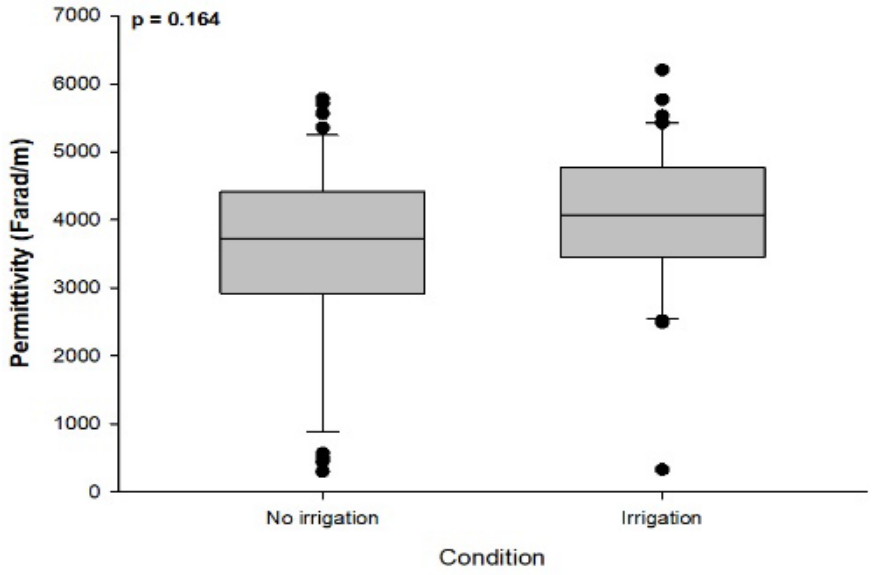

Figure 22: Permittivity of intracranial tumors at 200 kHz alternating electric fields with post-excised tissue (no irrigation) and irrigation with 0.9% NaCl saline solution for 5-10

4.4 Histological analysis of GBM tissue

The histological analysis demonstrated that the total cellularity and amount of myelin present in the brain tumor tissue might play a role in determining the dielectric properties of the tissue. GBM tissue from the same patient demonstrated that part with lower conductivity had higher myelin content and lower cellularity, while part with higher conductivity had low myelin content and higher cellularity (Figure 23).

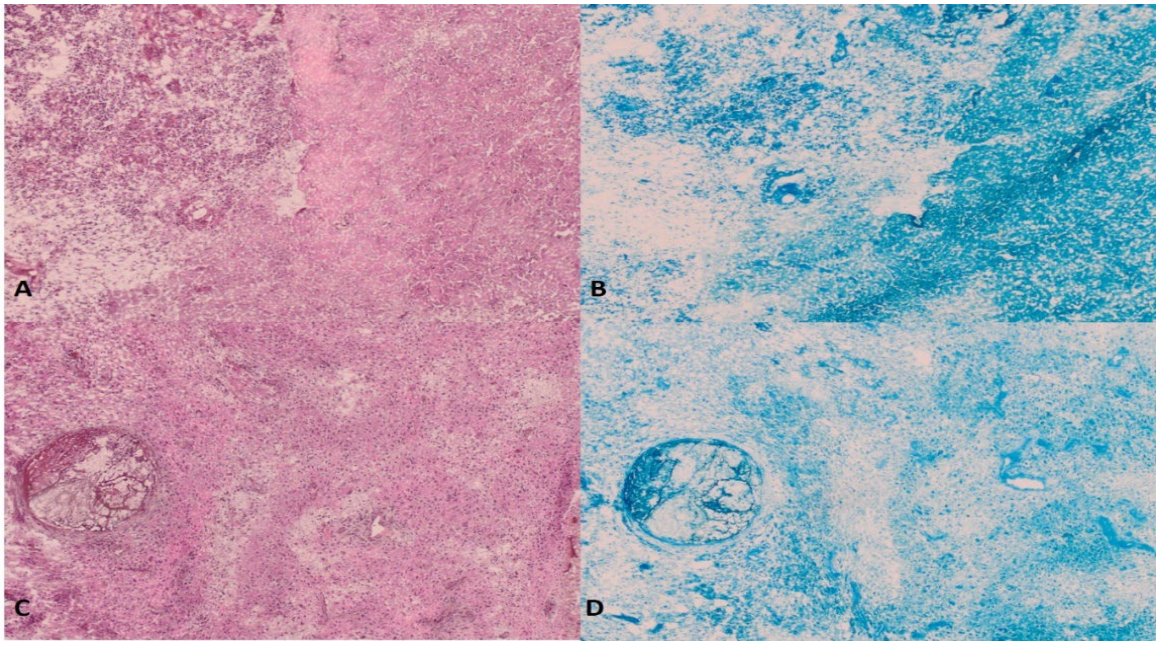

Figure 23: H&E (left side) and LFB (right side) staining of two different sites of GBM tissue from the same patient. A&B is one site and C&D is the second site. A&B showing high myelin and low cellularity while C& D are showing higher cellularity and lower myelin content. Images taken at 4x.

5. Discussion

The efficacy of TTFields depended on its electric field intensity in the GBM tissue. The intensity of TTFields is affected by tissue properties which further influence its dielectric properties [69]. The dipole moments of structural proteins that experience rotational forces within TTFields, and irregular aggregation of polarizable particles due to TTFields play a key role in the mechanism of action of this therapy [58, 59]. Therefore, it is of value to understand the main constituents of biological tissue, which give rise to the dielectric properties.

These main constituents are electrolytes, proteins, cell membrane and water content. Electrolytes are dissolved ionic compounds such as acids, bases and salts in water. The effects of these dissolved ions on the permittivity of biological tissue arises from producing a local electric field that effect the orientation of water molecules by reducing the way they can rotate in response to an applied electric field. Therefore, dissolved electrolytes lead to decrement in the permittivity of biological tissues [130]. The electrolytes also play role of charged particles, and the conductivity of biological tissue arises from the motion of these charged particles under the applied electric field. Therefore, electrolytes lead to decrement of permittivity and increment of conductivity in a biological material [131]. The conductivity is directly proportional to the valency, concentration, and electric mobility of each dissolved charged particle in the tissue. The pH can influence the concentration of the charged particles present in the tissue by dissociating water molecule into hydrogen ion (H^+) and hydroxyl ion (OH^-) at lower or higher pH. Thereby, pH can increase the conductivity in acidic and basic environment of the biological tissue [130]. Increased in conductivity was also observed in our study when tumor tissues were irrigated with 0.9% NaCl saline solution for 5-10 minutes, owing to increased concentration of charged ions (Na^+ and Cl^-) in the tissues.

The electric mobility of charged particles increases with increasing temperature. Hence, the conductivity of biological tissue is increased with the temperature [130]. Ryan et al. reported that electrical conductivity of brain tissue at 500 kHz increased with increasing temperature from 40 to 90 °C, and irreversible changes were observed above 60 °C [132]. A general increase of about 2% per °C occurs in the conductivity of tissue in the frequency range below 1 GHz [133]. Our results showed no significant change in conductivity of tumor tissue when it was heated from room temperature to

35 °C. The conductivity of tissue is increased with the temperature due to decrease in viscosity of the extracellular fluid and cytosol: thereby, charged particles can easily move through the tissue [133]. In our study design, the tissues were already placed in rigid holes when heating up the tissue, which could have prevented the expansion of the tissues due to change in viscosity. This in turn could have hindered the increased motility of charged particles that otherwise is observed with increasing temperature. However, other ex vivo studies done at 5-500 MHz have also shown no difference in the values of conductivity and permittivity of human gliomas at 24 °C to those of rat gliomas measured at 37 °C [124]. In addition, another study did not detect any difference observed in dielectric values of rat glioma at 37 °C and 43 °C [125] .

Proteins are made of one or more polypeptide chains, which are in turn made up of amino acids. The polypeptide chains are connected with each other through peptide bonds. These polypeptide chains fold into a specific configuration to give rise to three-dimensional structure of proteins. The amine ($–NH_2$) and carboxyl (–COOH) functional groups of amino acids at neutral pH exist in a zwitterion or dipolar ion (carboxylate ion (COO^-) and ammonium ion ($NH3^+$)), which are polarized under external electric field to give rise to a dipole moment. The dipole moment per unit volume of an amino acid is larger than that of a water molecule, so that the amino acids or protein solution has a greater permittivity than that of pure water [130]. Therefore, amino acids or proteins by replacing water molecules in a solution will lead to increased permittivity. The extent at which the dipole moments in proteins contribute to the permittivity depends on if they are free to rotate without any hindrance in applied electric field. Further, not all dipole moments that are free to rotate may contribute to the permittivity because it depends whether the dipoles are vectorially additive or cancelling [130]. These both factors, ability of dipole moments to rotate freely and vectorially additive, are influenced by the structural configuration of polypeptides in a protein.

Increased or decreased expression of proteins in a tissue, and the factors such as temperature and pH, which can change the structural configuration of proteins can influence the dielectric properties of the tissue [130]. Increasing temperature provides thermal energy to the dipoles, which in turn, randomize them. Thus, the number of dipoles that remain aligned in the direction of applied electric field become less, resulting in a lower permittivity [134]. However, our measurements showed no significant change in the permittivity of tumor tissues after increasing their temperature; although,

the decrease in permittivity in various biological tissues with increasing temperature has been reported by Rossmann et al. [135].

Cell membrane is composed of phospholipid bilayer with incorporated protein molecules. The phospholipid bilayers act as good insulators, and therefore provide the dominant resistive component of biological tissues, especially at lower frequencies. The phospholipid bilayers are also not readily polarizable, so they don't contribute much to the permittivity [130]. Further, the protein molecules in membranes are unable to contribute their intrinsically large dipole moments to the overall polarizability of the membrane due to rotational hindrance by the surrounding lipids [130]. In white matter of the brain, myelin sheath which is rich in lipid content also act as an insulator and provide resistance to the movement of charged particles. In fact, our results from histological analysis showed that the higher myelin content was correlated to lower conductivity in the GBM tissue.

The inside and the outside of the cell have solutions with dissolved ions, therefore, inside, and outside of the cell act as conductors separated by an insulator, the phospholipid membrane. This structural composition allows cell membrane to have capacitance, and it also makes it possible to have different amounts of electrical charges inside and outside the cell to create a potential difference across the membrane, so-called membrane potential. The membrane potential is important for the dielectric properties of the tissue, especially at lower frequencies [130]. Although the resistance and capacitance of the cell membrane hinder conductivity, it still remains high across cell membrane due to presence of ion channel proteins. Moreover, the presence of fluctuating proton populations due to hydration of membrane-bound proteins play a role in conductivity [131]. Therefore, the physiological process which control the transport of ions across the membrane influence the conductivity of the biological tissue [130]. A study has shown that the conductivity and permittivity dropped significantly after loss of the integrity and physiological viability of the cell membranes [136]; therefore, cell membrane is vital for dielectric properties of tissue at lower to intermediate frequency range [130]. This was also observed in our histological analysis of GBM tissue from the same patient, which showed that the tumor area with high number of intact cells with membranes had higher conductivity as compared to area with lower cellularity at frequency of 200 kHz (Figure 24).

Water content plays a key role in determining dielectric properties of the biological tissue. Water molecule can be easily polarized and exhibit a large dipole moment when an electric field is applied; therefore, contributing greatly to the permittivity of the tissue. However, it is important to differentiate between free water and bound water to proteins, while the bound water has hindered rotational ability as compared to the normal bulk water. Thereby, the bound water decreases the permittivity while bulk water increases it [137]. The dissociation of water molecule produces H^+ and OH^- ions; however, H^+ ions do not exist to significant amount in aqueous solution since they rapidly become hydrated through proton transfer to the hydronium ion (H_3O^+) which has very high motility similar to a proton. Therefore, H^+ and H_3O^+ have very high conductivity compared to any other ion present in biological tissue (147). Results from our experiments also demonstrated that the conductivity was significantly increased by irrigating the tumor tissues with saline solution, and when tumor tissues were dehydrated under laminar flow; the conductivity and permittivity of tumor tissues was reduced drastically.

It is important to understand which physiological elements play role in determining the dielectric properties of biological tissue at various frequencies of the applied electric field. The permittivity typically decreases with increasing frequency in three main steps which are known as α, β, and γ dispersions (Figure 24). These dispersions are caused by polarization of various cellular and molecular components. The α dispersion occurs below 10 kHz due to polarization of counterion layer along the cell membrane [131], β dispersion take place at frequencies between 10 kHz to 10 MHz due to polarization of cellular membranes, proteins and other organic macromolecules [138]; γ dispersion arises at frequencies above 10 GHz due to polarization of water molecules [139].

The conductivity of biological tissue increases with increasing frequency, and also corresponds to α, β, and γ dispersions (Figure 24). This is because the total conductivity is driven by two components: ionic conduction that is increased with increasing frequency and conduction caused by the energy produced due to the relaxation of polarized cellular and molecular components in α, β, and γ dispersions [130]. The frequency of TTFields (200 kHz) falls in the β dispersion where the cellular membrane is polarized and capacitive reactance short-circuits the membrane resistance, so the external electric field begins to penetrate into the cell interior. The relative importance of the permittivity and conductivity in determining the electrical properties of the tissue can be compared by taking the ratio of the currents caused by permittivity and conductivity; called

displacement current and conduction current respectively. For frequencies below MHz range, this ratio is very low, even with the large values of permittivity at these frequencies [133]. Hence, at TTFields frequency of 200 KHz, biological tissue is essentially conductive in nature [103]. This also provides the basis for mechanism of action of TTFields. Figure 24 shows the dielectric properties of normal biological tissues as compared to frequency, and dielectric properties of GBM tissue from our study at TTFields frequency [131, 133].

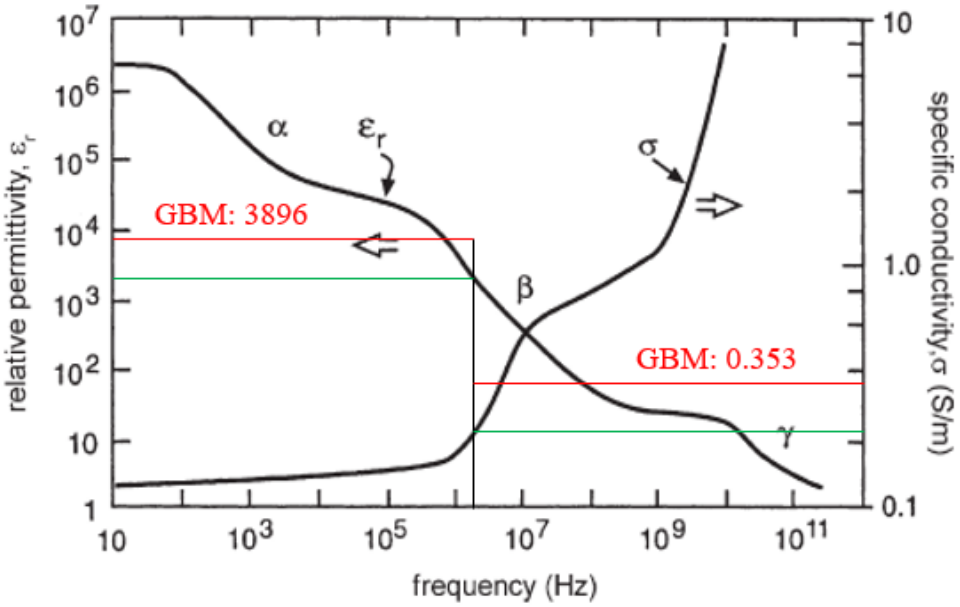

Figure 24: The GBM tissue has higher conductivity and permittivity as compared to normal biological tissue at 200 kHz.

The GBM tissue has higher electric properties than normal biological tissue at TTFields frequency. Previous studies have also demonstrated that the GBM tissue has higher values of conductivities as compared to the normal brain tissue at 50 kHz and 5-500 MHz [124, 140, 141]. The tumor tissue in general has higher dielectric properties than normal tissue due to different cellular composition [126, 142]. The structural and soluble proteins extracted from cancerous tissue exhibit a significantly larger relative permittivity and conductivity than that for similar proteins extracted from normal tissue [143]. The tumor tissue also has larger relaxation times in MRI, indicating a significant increase in the motional freedom of water [144]. The water content and sodium concentration in tumor cells is reported to be higher than in normal cells [124, 145], and also the cancer cells have reduced membrane potential [146]. The cancerous tissue is

shown to be more electronegative than normal tissues [147]. This is similar to the regenerative tissue, which is also electronegative and less differentiated [148].

Tumor angiogenesis is necessary for tumor progression. Tumor blood vessels provide nutrition and oxygen, and get rid of waste from tumor tissue, resulting in tumor progression. Tumor blood vessels have been shown to differ from their normal counterparts genetically and morphologically [149]. Tumor vasculature shows lack of arteriole-capillary-venule hierarchy and exhibit chaotic blood flow [149]. In GBM, tumor vessel exhibits loss of endothelial junctions and abrogated pericyte layer resulting in dysfunctional blood brain barrier (BBB) [150]. Hypoxia is a hallmark of GBM [151]. In hypoxic tissue osmosis will cause cell swelling and the extracellular pathways become narrow, which typically leads to decrease in conductivity [133]. On the other side, the mean cerebral blood volume (CBV) is reported to be higher in GBM tissue as compared to the normal brain tissue [152]. Blood is reported to be a very good conductor [131]. Therefore, this implies that GMB tissue has higher conductivity as compared to the normal brain tissue.

A defining hallmark of glioblastoma is altered tumor metabolism. The metabolic shift towards aerobic glycolysis with reprogramming of mitochondrial oxidative phosphorylation, regardless of oxygen availability, is a phenomenon known as the Warburg effect. In addition to the Warburg effect, glioblastoma tumor cells also utilize the tricarboxylic acid cycle/oxidative phosphorylation in a different capacity than normal tissue [153]. Increased lactic acid production as a result of aerobic glycolysis is reported in microenvironment of GBM, which is associated with poor survival and advanced disease [154]. As a consequence of such amounts of lactic acid there is an acidification of the extracellular pH in tumor microenvironment, ranging between 6.0 and 6.5. This acidosis favours processes such as metastasis, angiogenesis and more importantly, immunosuppression, which has been associated to a worse clinical prognosis [155]. The acidic pH can increase the conductivity in microenvironment of the biological tissue [130]. Therefore, this further supports the results of our study.

Histologically GBM consist of very heterogeneous tissue consisting of pleomorphic cells, varying mitotic activity, microvasculature, micro-thrombi, and necrosis with tumor cysts. This was reflected in our results, which demonstrated high inter- and intra-heterogeneous dielectric properties in the GBM patients. Moreover, the reason of this

heterogeneity among GBM patients could be due to different developmental stage of the tumor at the time of surgical resection and patients age [156]. Our results are in line with previous *in vivo* studies performed at 50 kHz, which have shown high variability in dielectric properties of GBM tissue, and also that the high grade gliomas have higher conductivities than lower grade gliomas [140, 156].

At the time of diagnosis, large central cystic lesions are encountered in 7% to 13% of GBM cases [157]. The central cystic lesion with high liquid content are also known as necrotic core of GBM, which contain liquefied dead cellular products or necrotic tissue, exudative plasma proteins from adjacent highly permeable vasculature, proliferative factors secreted by the tumor cells or mere trapping of CSF [157-159]. The necrotic core is known to have high levels of lactate probably on account of aerobic glycolysis with production of lactate by the tumor [159]. The conductivity of necrotic core is expected to be high due to its higher water content [160]. *In vivo* studies carried out at 50 kHz have shown higher conductivities of necrotic core as compared to solid part of the GBM tissue [140, 156, 160]. However, no *ex vivo* study has been carried out to date in order to determine the dielectric properties of the necrotic tissue present in the necrotic core. In our study, for the first time an attempt was made to measure directly the dielectric properties of the necrotic tissue present in the necrotic core. Our results showed statistically significant lower conductivity and permittivity of the necrotic tissue present in GBM necrotic core as compared to the solid part of the tumor. The loss of integrity and physiological viability of the cell membranes can lead to decrease in dielectric properties of the tissue at lower frequencies [130]. Therefore, it is possible that the necrotic tissue present in the necrotic core has lower conductivity and permittivity than the solid tumor tissue. However, the dielectric properties of the necrotic core when including both the dead tissue and fluid is higher due to the fluid content.

High variability in dielectric properties is also seen in other types of cancerous tissues, including hepatic and breast cancer tissues [142, 161]. Our results also demonstrated high variability in dielectric properties of all the intracranial tumors, including low grade gliomas, meningioma, and metastases. Meningioma exhibited the lowest variability when comparing with other intracranial tumors, and in fact could be differentiated from gliomas and metastases on the basis of their conductivity. This establishes that the dielectric properties reflect the tissue composition, because a meningioma is slow growing tumor with well demarcated borders and tissue is less heterogeneous than

gliomas and metastases [162]. However, the dielectric properties of tumors cannot be generalized due to high variability exist between different tumor types and even between tumors of the same type; therefore, dielectric properties can be useful to differentiate tumor lesions from the normal surrounding tissue, but diagnosing a specific tumor type might not be effective.

The understanding of intracranial distribution and intensity of TTFields is very important for effective treatment of GBM using TTFields. Computational modelling studies have calculated the TTFields distribution and intensity in the brain and in virtually introduced tumors of various sizes, shapes and locations in the brain using the values of dielectric properties shown in Table 1 [69, 74, 100, 103, 105, 163, 164]. The results of these studies have shed light on factors that are influencing the intracranial distribution and intensity of TTFields. Wenger et al. validated that at TTFields frequency, the conductivity of the tissues determines the TTFields distribution and intensity as compared to the permittivity [103]. The local field distribution induced by TTFields is largely determined by topographical conductivity variations in the tissue, because regions of local field enhancement were observed near interfaces between tissues with different topographical conductivities [69, 100]. This is because according to equation (6), the current induced by the TTFields first follows the path of tissues with higher conductivity and when it encounters tissue with lower conductivity, the higher number of charges are deposited at this interface; thus, creating higher TTFields intensity in tissues with lower conductivity at the interfaces [69].

The above mentioned effect was observed mainly at three anatomical interfaces in the brain [69, 100, 105]. Firstly, the high conductivity of CSF created a preferred pathways for current flow causing shunting of current through the CSF space, sulci and ventricles, and leading the current into less conductive tissue, such as the sulcal fundi, where high intensity of TTFields was observed [69]. Secondly, this effect was also valid for electric field strength in tumor tissue, where relatively high conductive tumor tissue created preferred pathway for current flow, when surrounded by normal brain tissue with a lower conductivity. This led the current to reach lower conductivity tissue, such as WM; thereby, causing high TTFields intensity in WM. This effect was pronounced when the current flow was perpendicular to the main WM fiber orientation [69]. This is because WM conductivity depends on anisotropy, where conductivity is higher longitudinally as compared to cross-sectional. Moreover, presence of central necrotic core

with high conductivity values as compared to the surrounding solid tumor also created preferred pathway for the current flow and caused the field strength to be unevenly distributed in the tumor volume with focal field enhancement at tumor boundaries perpendicular to the current; on the other side, homogeneous tumors experienced a more uniform field distribution throughout the entire volume [69, 105]. Thirdly, high TTFields intensity was also observed between the interfaces of gray matter with higher conductivity and WM with lower conductivity [69, 100, 105]. Therefore, the challenge remains to achieve threshold intensity of TTFields in GBM tissue with higher conductivity as compared to the surrounding tissue.

These computational modeling studies provided useful insight into understanding the mechanism with which TTFields are distributed in the brain and tumor tissue. Information derived from these studies can give clinicians an institutive understanding of the TTFields distribution in the brain for individual patients, and possibly predict where local recurrence may occur. For example, the efficiency of LR field directions is higher for tumors embedded in the deep white matter tracts whereas the efficiency of AP field directions is higher for tumors in the subcortical regions [69]. However, these modelling studies have limitations, including effect of other intracranial structures such as venous and atrial vasculature on TTFields distribution is not evaluated and these computational models are based on healthy subjects without any tumor pathology. Furthermore, lack of reliable values for dielectric properties of GBM at TTFields frequency from the literature may have affected the results and conclusions [69, 103].

Our study provided for the first time reliable dielectric values for GBM at TTFields frequency, which not only can be used in computational modeling to better understand the intracranial distribution of TTFields, but also can be used in NovoTAL system to predict effective placement of transducer arrays to maximize TTFields intensity in the tumor. The higher the intratumoral conductivity the lower the field intensity! There are limitations to our study, such as possible change in the geometry and physiological conditions of the tumor tissues, importantly water content. However, specially designed apparatus and fast acquisition protocol to obtain tumor tissues from the operation theater have utilized to minimize such artifacts to arise in the results. Alternative to *in vitro* method to measure dielectric properties of the tumor tissue is *in vivo* measurements. However, previous *in vivo* studies [127, 156] which measured resistivity of brain tumors

at 50 kHz have reported that taking measurements during surgical procedures is challenging and brings restrictive elements to the study. Furthermore, bleeding, saline wash, and leakage of CSF also influence the dielectric properties, and anesthesia decreases the volume of blood and CSF in the brain which further effect the values taken during surgical procedures. Due to physiological changes during operating conditions, it was observed that the conductivity of GM increased during the operations up to 100% [127].

One aspect that both our study and previous *in vivo* studies lack is anisotropy in dielectric measurements values. The conductivity of WM is anisotropic, which also plays role in intracranial distribution and intensity of TTFs [69]. Wenger et al. [103] calculated anisotropic conductivity values of normal brain tissues using diffusion tensor imaging (DTI) MRI with assumption that the conductivity tensors share the same eigenvectors as the effective diffusion tensor [165]. Using these anisotropic values of conductivity, it was observed that the TTFields intensity is increased around 10% in the tumor tissue [103]. The anisotropic conductivity values of GBM in patients suffering from this disease could also be calculated using DTI-MRI. Since our results demonstrated that high inter- and intra-variability exist in conductivity of GBM, values obtained using DTI-MRI would be of great value as they will account for heterogeneity in each patient and can also avoid the effects of artifacts on *in vitro* and *in vivo* measurement of conductivity. Moreover, comparing our values of conductivity with the DTI-MRI estimates of conductivity could further provide validation of both procedures. This could further lead to optimization of TTFields treatment.

6. Conclusion

TTFields have emerged as a non-invasive adjuvant therapy for newly diagnosed and recurrent GBM, which otherwise has a very poor prognosis. EF-14 clinical trial showed that the treatment of newly diagnosed GBM with TTFields plus TMZ was associated with an increase in PFS and OS for three months respectively in all subgroups of patients, regardless of age, sex, KPS score, MGMT promoter methylation status, geographic region or extent of resection. The effectiveness of this treatment depends on the patient's compliance with the treatment, and distribution and intensity of TTFields within the brain and in the GBM tissue. The intensity of TTFields in the GBM is determined by the dielectric properties of the tumor tissue. However, there are no reliable

values of dielectric properties of GBM available at TTFields frequency of 200 kHz. Our study for the first time has determined the dielectric properties of GBM and other intracranial tumors, by using a specially designed method. The results of our study showed that the dielectric properties of GBM are very variable within the same tumor and between different tumors. Furthermore, it is essential to measure the dielectric properties of tumor tissue in conditions that are as similar as possible to the conditions in the body, otherwise artifacts, such as change in water content in tumor tissue, can affect the results. Our study suggests that due to high inter- and intra-heterogeneity in dielectric properties of GBM, it is better to calculate values from each individual patient possibly by using a non-invasive method based on DTI-MRI. These values could be more reliable for effective planning and outcome of the GBM treatment with TTFields. However, until the DTI-MRI based conductivity estimation for individual patient is achieved, the values of dielectric properties for GBM reported in this study could be used in the NovoTAL system for more effective treatment planning, and also in computational modeling studies to better understand the intracranial distribution of TTFields. Moreover, our study design provides a reliable tool to further investigate the dielectric properties of healthy and tumor tissues in a laboratory setting.

7. Appendix

7.1 List of tables

7.2 List of figures

8. References

1. Ohgaki, H., *Epidemiology of brain tumors.* Methods Mol Biol, 2009. **472**: p. 323-42.
2. Dolecek, T.A., et al., *CBTRUS statistical report: primary brain and central nervous system tumors diagnosed in the United States in 2005-2009.* Neuro-oncology, 2012. **14 Suppl 5**(Suppl 5): p. v1-v49.
3. Crocetti, E., et al., *Epidemiology of glial and non-glial brain tumours in Europe.* Eur J Cancer, 2012. **48**(10): p. 1532-42.
4. Omuro, A. and L.M. DeAngelis, *Glioblastoma and other malignant gliomas: a clinical review.* JAMA, 2013. **310**(17): p. 1842-50.
5. DeAngelis, L.M., *Brain tumors.* N Engl J Med, 2001. **344**(2): p. 114-23.
6. Fan, K.J. and G.H. Pezeshkpour, *Ethnic distribution of primary central nervous system tumors in Washington, DC, 1971 to 1985.* J Natl Med Assoc, 1992. **84**(10): p. 858-63.
7. Hottinger, A.F. and Y. Khakoo, *Update on the management of familial central nervous system tumor syndromes.* Curr Neurol Neurosci Rep, 2007. **7**(3): p. 200-7.
8. Rajaraman, P., et al., *Genome-wide association study of glioma and meta-analysis.* Hum Genet, 2012. **131**(12): p. 1877-88.
9. Bondy, M.L., et al., *Brain tumor epidemiology: consensus from the Brain Tumor Epidemiology Consortium.* Cancer, 2008. **113**(7 Suppl): p. 1953-1968.
10. Linos, E., et al., *Atopy and risk of brain tumors: a meta-analysis.* J Natl Cancer Inst, 2007. **99**(20): p. 1544-50.
11. Louis, D.N., et al., *The 2021 WHO Classification of Tumors of the Central Nervous System: a summary.* Neuro Oncol, 2021. **23**(8): p. 1231-1251.
12. Weller, M., et al., *Molecular neuro-oncology in clinical practice: a new horizon.* Lancet Oncol, 2013. **14**(9): p. e370-9.
13. Kaina, B., et al., *MGMT: key node in the battle against genotoxicity, carcinogenicity and apoptosis induced by alkylating agents.* DNA Repair (Amst), 2007. **6**(8): p. 1079-99.
14. Wick, W., et al., *MGMT testing--the challenges for biomarker-based glioma treatment.* Nat Rev Neurol, 2014. **10**(7): p. 372-85.
15. Hegi, M.E., et al., *MGMT gene silencing and benefit from temozolomide in glioblastoma.* N Engl J Med, 2005. **352**(10): p. 997-1003.

16. Lalezari, S., et al., *Combined analysis of O6-methylguanine-DNA methyltransferase protein expression and promoter methylation provides optimized prognostication of glioblastoma outcome.* Neuro Oncol, 2013. **15**(3): p. 370-81.
17. Spiegl-Kreinecker, S., et al., *O6-Methylguanine DNA methyltransferase protein expression in tumor cells predicts outcome of temozolomide therapy in glioblastoma patients.* Neuro-oncology, 2010. **12**(1): p. 28-36.
18. Mikkelsen, V.E., et al., *The histological representativeness of glioblastoma tissue samples.* Acta Neurochir (Wien), 2021. **163**(7): p. 1911-1920.
19. Blume, C., et al., *Extracranial glioblastoma with synchronous metastases in the lung, pulmonary lymph nodes, vertebrae, cervical muscles and epidural space in a young patient - case report and review of literature.* BMC Res Notes, 2013. **6**: p. 290.
20. Brat, D.J., et al., *Pseudopalisades in glioblastoma are hypoxic, express extracellular matrix proteases, and are formed by an actively migrating cell population.* Cancer Res, 2004. **64**(3): p. 920-7.
21. Brat, D.J. and E.G. Van Meir, *Vaso-occlusive and prothrombotic mechanisms associated with tumor hypoxia, necrosis, and accelerated growth in glioblastoma.* Lab Invest, 2004. **84**(4): p. 397-405.
22. Olar, A. and K.D. Aldape, *Using the molecular classification of glioblastoma to inform personalized treatment.* J Pathol, 2014. **232**(2): p. 165-77.
23. Yi, Y., et al., *Glioblastoma Stem-Like Cells: Characteristics, Microenvironment, and Therapy.* Front Pharmacol, 2016. **7**: p. 477.
24. Vollmann-Zwerenz, A., et al., *Tumor Cell Invasion in Glioblastoma.* Int J Mol Sci, 2020. **21**(6).
25. Forsyth, P.A. and J.B. Posner, *Headaches in patients with brain tumors: a study of 111 patients.* Neurology, 1993. **43**(9): p. 1678-83.
26. Glantz, M.J., et al., *Practice parameter: anticonvulsant prophylaxis in patients with newly diagnosed brain tumors. Report of the Quality Standards Subcommittee of the American Academy of Neurology.* Neurology, 2000. **54**(10): p. 1886-93.
27. Bradley, W.G., Jr., et al., *Comparison of CT and MR in 400 patients with suspected disease of the brain and cervical spinal cord.* Radiology, 1984. **152**(3): p. 695-702.

28. Omuro, A.M., et al., *Pitfalls in the diagnosis of brain tumours.* Lancet Neurol, 2006. **5**(11): p. 937-48.
29. AbdelFatah, M.A.R., et al., *Impact of extent of resection of newly diagnosed glioblastomas on survival: a meta-analysis.* Egyptian Journal of Neurosurgery, 2022. **37**(1): p. 3.
30. Tunthanathip, T. and S. Madteng, *Factors associated with the extent of resection of glioblastoma.* Precision Cancer Medicine, 2020. **3**.
31. Tunthanathip, T., et al., *Butterfly Tumor of the Corpus Callosum: Clinical Characteristics, Diagnosis, and Survival Analysis.* J Neurosci Rural Pract, 2017. **8**(Suppl 1): p. S57-s65.
32. Chaichana, K.L., et al., *The butterfly effect on glioblastoma: is volumetric extent of resection more effective than biopsy for these tumors?* J Neurooncol, 2014. **120**(3): p. 625-34.
33. Noh, J.H., et al., *Optimal treatment of leptomeningeal spread in glioblastoma: analysis of risk factors and outcome.* Acta Neurochir (Wien), 2015. **157**(4): p. 569-76.
34. Sanai, N., et al., *An extent of resection threshold for newly diagnosed glioblastomas.* J Neurosurg, 2011. **115**(1): p. 3-8.
35. Moliterno, J.A., T.R. Patel, and J.M. Piepmeier, *Neurosurgical approach.* Cancer journal (Sudbury, Mass.), 2012. **18**(1): p. 20-25.
36. Kuhnt, D., et al., *Correlation of the extent of tumor volume resection and patient survival in surgery of glioblastoma multiforme with high-field intraoperative MRI guidance.* Neuro Oncol, 2011. **13**(12): p. 1339-48.
37. Mehta, M.P., et al., *The American Society for Therapeutic Radiology and Oncology (ASTRO) evidence-based review of the role of radiosurgery for brain metastases.* Int J Radiat Oncol Biol Phys, 2005. **63**(1): p. 37-46.
38. Stupp, R., et al., *Radiotherapy plus Concomitant and Adjuvant Temozolomide for Glioblastoma.* New England Journal of Medicine, 2005. **352**(10): p. 987-996.
39. Malmström, A., et al., *Temozolomide versus standard 6-week radiotherapy versus hypofractionated radiotherapy in patients older than 60 years with glioblastoma: the Nordic randomised, phase 3 trial.* Lancet Oncol, 2012. **13**(9): p. 916-26.

40. Keime-Guibert, F., et al., *Radiotherapy for glioblastoma in the elderly.* N Engl J Med, 2007. **356**(15): p. 1527-35.
41. Wick, W., et al., *Temozolomide chemotherapy alone versus radiotherapy alone for malignant astrocytoma in the elderly: the NOA-08 randomised, phase 3 trial.* Lancet Oncol, 2012. **13**(7): p. 707-15.
42. Westphal, M., et al., *A phase 3 trial of local chemotherapy with biodegradable carmustine (BCNU) wafers (Gliadel wafers) in patients with primary malignant glioma.* Neuro Oncol, 2003. **5**(2): p. 79-88.
43. Wick, W., et al., *Lomustine and Bevacizumab in Progressive Glioblastoma.* N Engl J Med, 2017. **377**(20): p. 1954-1963.
44. Omuro, A.M., S. Faivre, and E. Raymond, *Lessons learned in the development of targeted therapy for malignant gliomas.* Mol Cancer Ther, 2007. **6**(7): p. 1909-19.
45. Nagpal, S., G. Harsh, and L. Recht, *Bevacizumab improves quality of life in patients with recurrent glioblastoma.* Chemother Res Pract, 2011. **2011**: p. 602812.
46. Gramatzki, D., et al., *Bevacizumab may improve quality of life, but not overall survival in glioblastoma: an epidemiological study.* Ann Oncol, 2018. **29**(6): p. 1431-1436.
47. Omuro, A., et al., *Phase II trial of continuous low-dose temozolomide for patients with recurrent malignant glioma.* Neuro-oncology, 2013. **15**(2): p. 242-250.
48. Perry, J.R., et al., *Phase II trial of continuous dose-intense temozolomide in recurrent malignant glioma: RESCUE study.* J Clin Oncol, 2010. **28**(12): p. 2051-7.
49. Wick, A., et al., *Efficacy and tolerability of temozolomide in an alternating weekly regimen in patients with recurrent glioma.* J Clin Oncol, 2007. **25**(22): p. 3357-61.
50. Lombardi, G., et al., *Regorafenib compared with lomustine in patients with relapsed glioblastoma (REGOMA): a multicentre, open-label, randomised, controlled, phase 2 trial.* Lancet Oncol, 2019. **20**(1): p. 110-119.
51. Wen, P.Y. and D.A. Reardon, *Progress in glioma diagnosis, classification and treatment.* Nature Reviews Neurology, 2016. **12**(2): p. 69-70.

52. Chaichana, K.L., et al., *Factors associated with survival for patients with glioblastoma with poor pre-operative functional status.* Journal of clinical neuroscience : official journal of the Neurosurgical Society of Australasia, 2013. **20**(6): p. 818-823.
53. Stupp, R., et al., *Effects of radiotherapy with concomitant and adjuvant temozolomide versus radiotherapy alone on survival in glioblastoma in a randomised phase III study: 5-year analysis of the EORTC-NCIC trial.* Lancet Oncol, 2009. **10**(5): p. 459-66.
54. Gallego, O., *Nonsurgical treatment of recurrent glioblastoma.* Current oncology (Toronto, Ont.), 2015. **22**(4): p. e273-e281.
55. Weller, M., et al., *Standards of care for treatment of recurrent glioblastoma--are we there yet?* Neuro Oncol, 2013. **15**(1): p. 4-27.
56. Stupp, R., et al., *LTBK-01: Prospective, multi-center phase III trial of tumor treating fields together with temozolomide compared to temozolomide alone in patients with newly diagnosed glioblastoma.* Neuro-Oncology, 2016. **18**(Suppl 6): p. i1-i1.
57. Stupp, R., et al., *NovoTTF-100A versus physician's choice chemotherapy in recurrent glioblastoma: a randomised phase III trial of a novel treatment modality.* European Journal of Cancer, 2012. **48**(14): p. 2192-202.
58. Kirson, E.D., et al., *Disruption of cancer cell replication by alternating electric fields.* Cancer Res, 2004. **64**(9): p. 3288-95.
59. Kirson, E.D., et al., *Alternating electric fields arrest cell proliferation in animal tumor models and human brain tumors.* Proceedings of the National Academy of Sciences of the United States of America, 2007. **104**(24): p. 10152-7.
60. Kirson, E.D., et al., *Chemotherapeutic treatment efficacy and sensitivity are increased by adjuvant alternating electric fields (TTFields).* BMC Med Phys, 2009. **9**: p. 1.
61. Kanner, A.A., et al., *Post Hoc analyses of intention-to-treat population in phase III comparison of NovoTTF-100A system versus best physician's choice chemotherapy.* Semin Oncol, 2014. **41 Suppl 6**: p. S25-34.
62. Wong, E.T., et al., *Dexamethasone exerts profound immunologic interference on treatment efficacy for recurrent glioblastoma.* British Journal of Cancer, 2015. **113**(11): p. 1642.

63. Wong, E.T., et al., *Response assessment of NovoTTF-100A versus best physician's choice chemotherapy in recurrent glioblastoma.* Cancer Med, 2014. **3**(3): p. 592-602.
64. Burri, S.H., et al., *The Evolving Role of Tumor Treating Fields in Managing Glioblastoma: Guide for Oncologists.* American journal of clinical oncology, 2018. **41**(2): p. 191-196.
65. Mrugala, M.M., et al., *Clinical practice experience with NovoTTF-100A system for glioblastoma: The Patient Registry Dataset (PRiDe).* Semin Oncol, 2014. **41 Suppl 6**: p. S4-S13.
66. Stupp, R., et al., *Effect of Tumor-Treating Fields Plus Maintenance Temozolomide vs Maintenance Temozolomide Alone on Survival in Patients With Glioblastoma: A Randomized Clinical Trial.* JAMA, 2017. **318**(23): p. 2306-2316.
67. Kinzel, A., et al., *Tumor Treating Fields for Glioblastoma Treatment: Patient Satisfaction and Compliance With the Second-Generation Optune(®) System.* Clinical Medicine Insights. Oncology, 2019. **13**: p. 1179554918825449-1179554918825449.
68. Fonkem, E. and E.T. Wong, *NovoTTF-100A: a new treatment modality for recurrent glioblastoma.* Expert Rev Neurother, 2012. **12**(8): p. 895-9.
69. Korshoej, A.R., et al., *Impact of tumor position, conductivity distribution and tissue homogeneity on the distribution of tumor treating fields in a human brain: A computer modeling study.* PLoS One, 2017. **12**(6): p. e0179214.
70. Vymazal, J. and E.T. Wong, *Response patterns of recurrent glioblastomas treated with tumor-treating fields.* Semin Oncol, 2014. **41 Suppl 6**: p. S14-24.
71. Rulseh, A.M., et al., *Long-term survival of patients suffering from glioblastoma multiforme treated with tumor-treating fields.* World J Surg Oncol, 2012. **10**: p. 220.
72. Villano, J.L., et al., *Delayed response and survival from NovoTTF-100A in recurrent GBM.* Med Oncol, 2013. **30**(1): p. 338.
73. Chaudhry, A., et al., *NovoTTF-100A System (Tumor Treating Fields) transducer array layout planning for glioblastoma: a NovoTAL system user study.* World J Surg Oncol, 2015. **13**: p. 316.

74. Wenger, C., et al., *Improving Tumor Treating Fields Treatment Efficacy in Patients With Glioblastoma Using Personalized Array Layouts.* International Journal of Radiation Oncology, Biology, Physics, 2015.
75. Au - Riley, M.M., et al., *The Clinical Application of Tumor Treating Fields Therapy in Glioblastoma.* JoVE, 2019(146): p. e58937.
76. Bomzon, Z., et al., *Modelling Tumor Treating Fields for the treatment of lung-based tumors.* Conf Proc IEEE Eng Med Biol Soc, 2015. **2015**: p. 6888-91.
77. Giladi, M., et al., *Alternating electric fields (tumor-treating fields therapy) can improve chemotherapy treatment efficacy in non-small cell lung cancer both in vitro and in vivo.* Seminars in Oncology, 2014. **41 Suppl 6**: p. S35-41.
78. Gera, N., et al., *Tumor Treating Fields Perturb the Localization of Septins and Cause Aberrant Mitotic Exit.* PLoS One, 2015. **10**(5): p. e0125269.
79. Mershin, A., et al., *Tubulin dipole moment, dielectric constant and quantum behavior: computer simulations, experimental results and suggestions.* Biosystems, 2004. **77**(1-3): p. 73-85.
80. Giladi, M., et al., *Mitotic Spindle Disruption by Alternating Electric Fields Leads to Improper Chromosome Segregation and Mitotic Catastrophe in Cancer Cells.* Sci Rep, 2015. **5**: p. 18046.
81. Albertson, R., et al., *Vesicles and actin are targeted to the cleavage furrow via furrow microtubules and the central spindle.* The Journal of cell biology, 2008. **181**(5): p. 777-790.
82. D'Avino, P.P., M.S. Savoian, and D.M. Glover, *Cleavage furrow formation and ingression during animal cytokinesis: a microtubule legacy.* J Cell Sci, 2005. **118**(Pt 8): p. 1549-58.
83. Rankin, K.E. and L. Wordeman, *Long astral microtubules uncouple mitotic spindles from the cytokinetic furrow.* Journal of Cell Biology, 2010. **190**(1): p. 35-43.
84. Field, C.M., et al., *Characterization of anillin mutants reveals essential roles in septin localization and plasma membrane integrity.* Development, 2005. **132**(12): p. 2849-60.
85. Gilden, J.K., et al., *The septin cytoskeleton facilitates membrane retraction during motility and blebbing.* J Cell Biol, 2012. **196**(1): p. 103-14.
86. Gilden, J. and M.F. Krummel, *Control of cortical rigidity by the cytoskeleton: Emerging roles for septins.* Cytoskeleton, 2010. **67**(8): p. 477-486.

87. Huang, H.C., et al., *Evidence that mitotic exit is a better cancer therapeutic target than spindle assembly.* Cancer Cell, 2009. **16**(4): p. 347-58.
88. Margolis, R.L., O.D. Lohez, and P.R. Andreassen, *G1 tetraploidy checkpoint and the suppression of tumorigenesis.* J Cell Biochem, 2003. **88**(4): p. 673-83.
89. Ganem, N.J. and D. Pellman, *Limiting the Proliferation of Polyploid Cells.* Cell, 2007. **131**(3): p. 437-440.
90. Davies, A.M., U. Weinberg, and Y. Palti, *Tumor treating fields: a new frontier in cancer therapy.* Ann N Y Acad Sci, 2013. **1291**: p. 86-95.
91. Tuszynski, J.A., et al., *An Overview of Sub-Cellular Mechanisms Involved in the Action of TTFields.* Int J Environ Res Public Health, 2016. **13**(11).
92. Senovilla, L., et al., *An immunosurveillance mechanism controls cancer cell ploidy.* Science, 2012. **337**(6102): p. 1678-84.
93. Kepp, O., et al., *Immunogenic cell death modalities and their impact on cancer treatment.* Apoptosis, 2009. **14**(4): p. 364-75.
94. Kepp, O., et al., *Consensus guidelines for the detection of immunogenic cell death.* Oncoimmunology, 2014. **3**(9): p. e955691.
95. Kirson, E.D., et al., *Alternating electric fields (TTFields) inhibit metastatic spread of solid tumors to the lungs.* Clin Exp Metastasis, 2009. **26**(7): p. 633-40.
96. Kim, E.H., et al., *Tumor treating fields inhibit glioblastoma cell migration, invasion and angiogenesis.* Oncotarget, 2016. **7**(40): p. 65125-65136.
97. Kim, E.H., et al., *Biological effect of an alternating electric field on cell proliferation and synergistic antimitotic effect in combination with ionizing radiation.* Oncotarget, 2016. **7**(38): p. 62267-62279.
98. Karanam, N.K., et al., *Tumor-treating fields elicit a conditional vulnerability to ionizing radiation via the downregulation of BRCA1 signaling and reduced DNA double-strand break repair capacity in non-small cell lung cancer cell lines.* Cell Death Dis, 2017. **8**(3): p. e2711.
99. Louis, D.N., et al., *The 2016 World Health Organization Classification of Tumors of the Central Nervous System: a summary.* Acta Neuropathologica, 2016. **131**(6): p. 803-820.
100. Wenger, C., et al., *A review on Tumor Treating Fields (TTFields): Clinical implications inferred from computational modeling.* IEEE Rev Biomed Eng, 2018.

101. Toms, S.A., et al., *Increased compliance with tumor treating fields therapy is prognostic for improved survival in the treatment of glioblastoma: a subgroup analysis of the EF-14 phase III trial.* Journal of Neuro-Oncology, 2019. **141**(2): p. 467-473.
102. Lacouture, M.E., et al., *Characterization and management of dermatologic adverse events with the NovoTTF-100A System, a novel anti-mitotic electric field device for the treatment of recurrent glioblastoma.* Seminars in Oncology, 2014. **41 Suppl 4**: p. S1-14.
103. Wenger, C., et al., *The electric field distribution in the brain during TTFields therapy and its dependence on tissue dielectric properties and anatomy: a computational study.* Physics in Medicine and Biology, 2015. **60**(18): p. 7339-57.
104. Miranda, P.C., et al., *Predicting the electric field distribution in the brain for the treatment of glioblastoma.* Physics in medicine and biology, 2014. **59**(15): p. 4137-4147.
105. Lok, E., et al., *Analysis of physical characteristics of Tumor Treating Fields for human glioblastoma.* Cancer Med, 2017. **6**(6): p. 1286-1300.
106. Grimnes, S. and Ø.G. Martinsen, *Chapter 1 - Introduction*, in *Bioimpedance and Bioelectricity Basics (Third Edition)*, S. Grimnes and Ø.G. Martinsen, Editors. 2015, Academic Press: Oxford. p. 1-7.
107. Grimnes, S. and Ø.G. Martinsen, *Chapter 4 - Passive Tissue Electrical Properties*, in *Bioimpedance and Bioelectricity Basics (Third Edition)*, S. Grimnes and Ø.G. Martinsen, Editors. 2015, Academic Press: Oxford. p. 77-118.
108. Gabriel, S., R.W. Lau, and C. Gabriel, *The dielectric properties of biological tissues: III. Parametric models for the dielectric spectrum of tissues.* Phys Med Biol, 1996. **41**(11): p. 2271-93.
109. Hemingway, A. and J.F. McClendon, *THE HIGH FREQUENCY RESISTANCE OF HUMAN TISSUE.* American Journal of Physiology-Legacy Content, 1932. **102**(1): p. 56-59.
110. Yamamoto, T. and Y. Yamamoto, *Electrical properties of the epidermal stratum corneum.* Medical and Biological Engineering, 1976. **14**(2): p. 151-8.

111. Burger, H.C. and J.B. van Milaan, *Measurement of specific resistance of the human body to direct current.* Acta Medica Scandinavica, 1943. **114**: p. 584-607.
112. De Mercato, G. and F.J. Garcia Sanchez, *Correlation between low-frequency electric conductivity and permittivity in the diaphysis of bovine femoral bone.* IEEE Trans Biomed Eng, 1992. **39**(5): p. 523-6.
113. Kosterich, J.D., K.R. Foster, and S.R. Pollack, *Dielectric permittivity and electrical conductivity of fluid saturated bone.* IEEE Trans Biomed Eng, 1983. **30**(2): p. 81-6.
114. Reddy, G.N. and S. Saha, *Electrical and dielectric properties of wet bone as a function of frequency.* IEEE Trans Biomed Eng, 1984. **31**(3): p. 296-303.
115. Law, S.K., *Thickness and resistivity variations over the upper surface of the human skull.* Brain Topogr, 1993. **6**(2): p. 99-109.
116. Baumann, S.B., et al., *The electrical conductivity of human cerebrospinal fluid at body temperature.* IEEE Trans Biomed Eng, 1997. **44**(3): p. 220-3.
117. Crile, G.W., H.R. Hosmer, and A.F. Rowland, *THE ELECTRICAL CONDUCTIVITY OF ANIMAL TISSUES UNDER NORMAL AND PATHOLOGICAL CONDITIONS.* American Journal of Physiology-Legacy Content, 1922. **60**(1): p. 59-106.
118. Logothetis, N.K., C. Kayser, and A. Oeltermann, *In vivo measurement of cortical impedance spectrum in monkeys: implications for signal propagation.* Neuron, 2007. **55**(5): p. 809-23.
119. Ranck, J.B., Jr., *Specific impedance of rabbit cerebral cortex.* Exp Neurol, 1963. **7**: p. 144-52.
120. Gabriel, C., A. Peyman, and E.H. Grant, *Electrical conductivity of tissue at frequencies below 1 MHz.* Physics in Medicine and Biology, 2009. **54**(16): p. 4863-78.
121. Stoy, R.D., K.R. Foster, and H.P. Schwan, *Dielectric properties of mammalian tissues from 0.1 to 100 MHz: a summary of recent data.* Physics in Medicine and Biology, 1982. **27**(4): p. 501-13.
122. Surowiec, A., S.S. Stuchly, and A. Swarup, *Postmortem changes of the dielectric properties of bovine brain tissues at low radiofrequencies.* Bioelectromagnetics, 1986. **7**(1): p. 31-43.

123. Van Harreveld, A., T. Murphy, and K.W. Nobel, *Specific impedance of rabbit's cortical tissue.* Am J Physiol, 1963. **205**: p. 203-7.
124. Lu, Y., et al., *Dielectric properties of human glioma and surrounding tissue.* International Journal of Hyperthermia, 1992. **8**(6): p. 755-60.
125. Peloso, R., D.T. Tuma, and R.K. Jain, *Dielectric properties of solid tumors during normothermia and hyperthermia.* IEEE Transactions on Biomedical Engineering, 1984. **31**(11): p. 725-8.
126. Surowiec, A.J., et al., *Dielectric properties of breast carcinoma and the surrounding tissues.* IEEE Transactions on Biomedical Engineering, 1988. **35**(4): p. 257-63.
127. Latikka, J., T. Kuurne, and H. Eskola, *Conductivity of living intracranial tissues.* Physics in Medicine and Biology, 2001. **46**(6): p. 1611-6.
128. Callegaro, L., *Electrical Impedance: Principles, Measurement, and Applications*. 2012: CRC Press. 308.
129. Böck, P., ed. *Romeis Mikroskopische Technik*. 17 ed. 1989, Urban und Schwarzenberg: München. 697.
130. Pethig, R., *Dielectric properties of body tissues.* Clin Phys Physiol Meas, 1987. **8 Suppl A**: p. 5-12.
131. Foster, K.R. and H.P. Schwan, *Dielectric properties of tissues and biological materials: a critical review.* Crit Rev Biomed Eng, 1989. **17**(1): p. 25-104.
132. Ryan, T.P., et al., *Tissue electrical properties as a function of thermal dose for use in a finite element model.* ASME-PUBLICATIONS-HTD, 1997. **355**: p. 167-172.
133. Miklavčič, D., N. Pavšelj, and F.X. Hart, *Electric Properties of Tissues*, in *Wiley Encyclopedia of Biomedical Engineering*. 2006, John Wiley & Sons, Inc.
134. Tripathi, M., et al., *Effect of temperature on dielectric properties and penetration depth of oil palm shell (OPS) and OPS char synthesized by microwave pyrolysis of OPS.* Fuel, 2015. **153**: p. 257-266.
135. Rossmanna, C. and D. Haemmerich, *Review of temperature dependence of thermal properties, dielectric properties, and perfusion of biological tissues at hyperthermic and ablation temperatures.* Critical reviews in biomedical engineering, 2014. **42**(6): p. 467-492.

136. Fricke , H. and H.J. Curtis *THE ELECTRIC IMPEDANCE OF HEMOLYZED SUSPENSIONS OF MAMMALIAN ERYTHROCYTES.* Journal of General Physiology, 1935. **18**(6): p. 821-836.
137. Buchanan, T.J., et al., *The Dielectric Estimation of Protein Hydration.* Proceedings of the Royal Society of London. Series A, Mathematical and Physical Sciences, 1952. **213**(1114): p. 379-391.
138. Schwan, H.P., *Electrical properties of tissue and cell suspensions.* Adv Biol Med Phys, 1957. **5**: p. 147-209.
139. Schwan, H.P., *ELECTRICAL PROPERTIES OF BLOOD AT ULTRAHIGH FREQUENCIES.* American Journal of Physical Medicine & Rehabilitation, 1953. **32**(3).
140. Rajshekhar, V., *Continuous impedance monitoring during CT-guided stereotactic surgery: relative value in cystic and solid lesions.* Br J Neurosurg, 1992. **6**(5): p. 439-44.
141. Bullard, D.E., *Intraoperative impedance monitoring during CT-guided stereotactic biopsies.* Stereotact Funct Neurosurg, 1989. **52**(1): p. 1-17.
142. Smith, S.R., K.R. Foster, and G.L. Wolf, *Dielectric properties of VX-2 carcinoma versus normal liver tissue.* IEEE Trans Biomed Eng, 1986. **33**(5): p. 522-4.
143. Gascoyne, P.R., R. Pethig, and A. Szent-Györgyi, *Water structure-dependent charge transport in proteins.* Proceedings of the National Academy of Sciences, 1981. **78**(1): p. 261.
144. Hazlewood, C.F., et al., *Nuclear magnetic resonance transverse relaxation times of water protons in skeletal muscle.* Biophys J, 1974. **14**(8): p. 583-606.
145. Damadian, R. and F.W. Cope, *NMR in cancer. V. Electronic diagnosis of cancer by potassium (39K) nuclear magnetic resonance: spin signatures and T1 beat patterns.* Physiol Chem Phys, 1974. **6**(4): p. 309-22.
146. Cone, C.D., Jr., *Electroosmotic interactions accompanying mitosis initation in sarcoma cells in vitro.* Trans N Y Acad Sci, 1969. **31**(4): p. 404-27.
147. Schauble, M.K. and M.B. Habal, *Electropotentials of tumor tissue.* J Surg Res, 1969. **9**(9): p. 517-20.
148. Becker, R.O., *The bioelectric factors in amphibian-limb regeneration.* J Bone Joint Surg Am, 1961. **43-a**: p. 643-56.

149. Hida, K., Y. Hida, and M. Shindoh, *Understanding tumor endothelial cell abnormalities to develop ideal anti-angiogenic therapies.* Cancer Science, 2008. **99**(3): p. 459-466.
150. Rosińska, S. and J. Gavard, *Tumor Vessels Fuel the Fire in Glioblastoma.* Int J Mol Sci, 2021. **22**(12).
151. Park, J.H. and H.K. Lee, *Current Understanding of Hypoxia in Glioblastoma Multiforme and Its Response to Immunotherapy.* Cancers (Basel), 2022. **14**(5).
152. Kim, H.S., et al., *Posttreatment high-grade glioma: usefulness of peak height position with semiquantitative MR perfusion histogram analysis in an entire contrast-enhanced lesion for predicting volume fraction of recurrence.* Radiology, 2010. **256**(3): p. 906-15.
153. Agnihotri, S. and G. Zadeh, *Metabolic reprogramming in glioblastoma: the influence of cancer metabolism on epigenetics and unanswered questions.* Neuro Oncol, 2016. **18**(2): p. 160-72.
154. Saraswathy, S., et al., *Evaluation of MR markers that predict survival in patients with newly diagnosed GBM prior to adjuvant therapy.* J Neurooncol, 2009. **91**(1): p. 69-81.
155. de la Cruz-López, K.G., et al., *Lactate in the Regulation of Tumor Microenvironment and Therapeutic Approaches.* Frontiers in Oncology, 2019. **9**.
156. Latikka, J. and H. Eskola, *The Resistivity of Human Brain Tumours In Vivo.* Ann Biomed Eng, 2019. **47**(3): p. 706-713.
157. Hoelscher, M., et al., *SELDI-TOF analysis of glioblastoma cyst fluid is an approach for assessing cellular protein expression.* Neurological research, 2013. **35**(10): p. 993-1001.
158. Westphal, M., H. Nausch, and H.D. Herrmann, *Cyst fluids of malignant human brain tumors contain substances that stimulate the growth of cultured human gliomas of various histological type.* Neurosurgery, 1989. **25**(2): p. 196-201.
159. Lohle, P.N.M., et al., *Analysis of Fluid in Cysts Accompanying Various Primary and Metastatic Brain Tumours: Proteins, Lactate and pH.* Acta Neurochirurgica, 1998. **140**(1): p. 14-19.
160. Bullard, D.E. and T.T. Makachinas, *Measurement of tissue impedence in conjunction with computed tomography-guided stereotaxic biopsies.* Journal of neurology, neurosurgery, and psychiatry, 1987. **50**(1): p. 43-51.

161. Haemmerich, D., et al., *In vivo electrical conductivity of hepatic tumours.* Physiol Meas, 2003. **24**(2): p. 251-60.
162. Shibuya, M., *Pathology and molecular genetics of meningioma: recent advances.* Neurologia medico-chirurgica, 2015. **55**(1): p. 14-27.
163. Wenger, C., et al., *Simplified realistic human head model for simulating Tumor Treating Fields (TTFields).* Conf Proc IEEE Eng Med Biol Soc, 2016. **2016**: p. 5664-5667.
164. Miranda, P.C., et al., *Predicting the electric field distribution in the brain for the treatment of glioblastoma.* Phys Med Biol, 2014. **59**(15): p. 4137-47.
165. Basser, P.J., J. Mattiello, and D. LeBihan, *MR diffusion tensor spectroscopy and imaging.* Biophys J, 1994. **66**(1): p. 259-67.

9. Acknowledgement

I would like to express my sincere gratitude to my mentor Prof. Dr. Martin Proescholdt for giving me the opportunity to work in his Laboratory and for his continuous support of my thesis, for his patience, motivation, and immense knowledge. I would also like to thank Eva-Maria Störr for her help in the laboratory work. I would also like to thank my family and friends for their unlimited support for my career.